Interpreting A and B metrics with Λ as gravitational field of a tachyon in an (anti–)de Sitter universe

O. Hruška[*] and J. Podolský[†]

Institute of Theoretical Physics, Charles University, V Holešovičkách 2, 18000 Prague 8, Czech Republic

We investigate the main properties and mutual relations of the so-called A and B metrics with any value of the cosmological constant. In particular, we explicitly show that both the *AII* and *BI* metrics are, in fact, the famous Schwarzschild–(anti–)de Sitter spacetime (that is the *AI* metric) boosted to superluminal speed. Together, they can be combined to form a complete gravitational field of a tachyon in an asymptotically Minkowski or (anti–)de Sitter background. The boundary separating the *AII* and *BI* regions is the Mach-Cherenkov shockwave on which the curvature is unbounded. We analyze various geometric features of such spacetimes, provide their natural physical interpretation, and visualize them using convenient background coordinates and embeddings.

I. INTRODUCTION

In a seminal work [1] published in 1962, Ehlers and Kundt systematically investigated static vacuum gravitational fields. In particular, they introduced a classification of all such fields of algebraic type D, denoting them as classes A and B (and also C, later interpreted physically as the metric in a static region around uniformly accelerating black holes [2]).

The A metrics, consisting of three subclasses, were written in Ref. [1] in the form[1]

$$AI: \ \mathrm{d}s^2 = r^2(\mathrm{d}\vartheta^2 + \sin^2\vartheta \mathrm{d}\varphi^2)$$
$$+ \left(1 - \frac{b}{r}\right)^{-1}\mathrm{d}r^2 - \left(1 - \frac{b}{r}\right)\mathrm{d}t^2, \quad (1)$$

$$AII: \ \mathrm{d}s^2 = z^2(\mathrm{d}r^2 + \sinh^2 r \mathrm{d}\varphi^2)$$
$$+ \left(\frac{b}{z} - 1\right)^{-1}\mathrm{d}z^2 - \left(\frac{b}{z} - 1\right)\mathrm{d}t^2, \quad (2)$$

$$AIII: \ \mathrm{d}s^2 = z^2(\mathrm{d}r^2 + r^2\mathrm{d}\varphi^2) + z\mathrm{d}z^2 - \frac{\mathrm{d}t^2}{z} \quad (3)$$

(see also Table 18.2 in Ref. [3] or Chapter 9 in Ref. [4]). The *AI* metric is the famous Schwarzschild solution [5] describing the external vacuum field of a spherically symmetric static object or black hole. The A metrics can

be generalized to include (for example) a cosmological constant Λ, and can be written in a unified form

$$\mathrm{d}s^2 = p^2(\epsilon_0 - \epsilon_2 q^2)\mathrm{d}\varphi^2 + \frac{p^2}{\epsilon_0 - \epsilon_2 q^2}\mathrm{d}q^2$$
$$- \left(\epsilon_2 + \frac{2n}{p} - \frac{\Lambda}{3}p^2\right)\mathrm{d}t^2 + \left(\epsilon_2 + \frac{2n}{p} - \frac{\Lambda}{3}p^2\right)^{-1}\mathrm{d}p^2. \quad (4)$$

For $\epsilon_2 = 1, -1, 0$, we obtain the *AI*, *AII* and *AIII* metrics, respectively, as indicated in Table I. The *AI* metric with Λ is the (so-called) Schwarzschild–de Sitter solution, first found by Kottler [6], and its standard form is obtained by setting $p = r$, $q = \cos\vartheta$, $n = -M$, $\epsilon_0 = 1$. The *AII* and *AIII* metrics have been described and studied as "topological black holes" (see, e.g., Ref. [4] for a list of references).

The B metrics were introduced in Ref. [1] in the form

$$BI: \ \mathrm{d}s^2 = \left(1 - \frac{b}{r}\right)^{-1}\mathrm{d}r^2 + \left(1 - \frac{b}{r}\right)\mathrm{d}\varphi^2$$
$$+ r^2(\mathrm{d}\vartheta^2 - \sin^2\vartheta \mathrm{d}t^2), \quad (5)$$

$$BII: \ \mathrm{d}s^2 = \left(\frac{b}{z} - 1\right)^{-1}\mathrm{d}z^2 + \left(\frac{b}{z} - 1\right)\mathrm{d}\varphi^2$$
$$+ z^2(\mathrm{d}r^2 - \sinh^2 r \mathrm{d}t^2), \quad (6)$$

$$BIII: \ \mathrm{d}s^2 = z\mathrm{d}z^2 + \frac{\mathrm{d}\varphi^2}{z} + z^2(\mathrm{d}r^2 - r^2\mathrm{d}t^2). \quad (7)$$

Although these metrics also look very simple and have been known for more than 50 years, they have not received as much attention as their counterparts (1)–(3).

---

[*]HruskaOndrej@seznam.cz
[†]podolsky@mbox.troja.mff.cuni.cz
[1]We distinguish three types of A and B metrics by roman numerals, instead of arabic numerals employed in Ref. [1].

Analogously to Eq. (4), it is possible to include any cosmological constant and write the B metrics in a unified form

$$ds^2 = -p^2(\epsilon_0 - \epsilon_2 q^2)dt^2 + \frac{p^2}{\epsilon_0 - \epsilon_2 q^2}dq^2$$
$$+ \left(\epsilon_2 + \frac{2n}{p} - \frac{\Lambda}{3}p^2\right)dz^2 + \left(\epsilon_2 + \frac{2n}{p} - \frac{\Lambda}{3}p^2\right)^{-1}dp^2.$$
$$\tag{8}$$

For the choices $\epsilon_2 = 1, -1, 0$, we obtain the BI, BII and BIII metrics, respectively, as also summarized in Table I. Moreover, as we demonstrated in Refs. [7,8], the parameter $\epsilon_0 = 1, -1, 0$ in both Eqs. (4) and (8) has *no physical meaning* because it only changes the specific coordinate foliation of the two-dimensional subspace covered by the φ, q and t, q coordinates, respectively. Without loss of generality we may thus choose any ϵ_0 to obtain the most suitable form of the metric.

The A metric (4) can further be generalized to include electromagnetic charges, rotation, a Newman-Unti-Tamburino parameter, and acceleration. Such generalized black holes are contained in the large Plebański–Demiański class [9] of *expanding* type D solutions; see Ref. [10] for more details. Interestingly, the C metric is then also naturally included in this Plebański–Demiański class.

Moreover, the B metrics can also be considered as a subcase of the Plebański–Demiański class of metrics in a *nonexpanding* limit in which the double-degenerate null congruence has zero expansion, shear and twist. Such a class has the form

$$ds^2 = \varrho^2\left(-\mathcal{Q}dt^2 + \frac{1}{\mathcal{Q}}dq^2\right) + \frac{\mathcal{P}}{\varrho^2}(dz + 2\gamma q dt)^2 + \frac{\varrho^2}{\mathcal{P}}dp^2,$$
$$\tag{9}$$

where

TABLE I.   Transformations between the unified form (4) of A metrics (upper part) or B metrics (8) (lower part) and the original forms (1)–(3) or (5)–(7), respectively, as presented by Ehlers and Kundt in the case when $\Lambda = 0$.

	ϵ_2	ϵ_0	φ	q	t	p	n	Equations
AI	1	1	φ	$\cos\vartheta$	t	r	$-b/2$	(4) → (1)
AII	−1	−1	φ	$\cosh r$	t	z	$b/2$	(4) → (2)
AIII	0	1	$r\sin\varphi$	$r\cos\varphi$	t	z	$1/2$	(4) → (3)

			t	q	z	p	n	Equations
BI	1	1	t	$\cos\vartheta$	φ	r	$-b/2$	(8) → (5)
BII	−1	−1	t	$\cosh r$	φ	z	$b/2$	(8) → (6)
BIII	0	1	$r\sinh t$	$r\cosh t$	φ	z	$1/2$	(8) → (7)

$$\varrho^2 = p^2 + \gamma^2, \qquad \mathcal{Q}(q) = \epsilon_0 - \epsilon_2 q^2,$$
$$\mathcal{P}(p) = (-(e^2 + g^2) - \epsilon_2\gamma^2 + \Lambda\gamma^4) + 2np$$
$$+ (\epsilon_2 - 2\Lambda\gamma^2)p^2 - \frac{1}{3}\Lambda p^4 \tag{10}$$

(see Sec. 16.4 in Ref. [4]). It contains two discrete geometrical parameters $\epsilon_0, \epsilon_2 = 1, -1, 0$, the cosmological constant Λ, electric and magnetic charges e and g, the masslike parameter n, and an additional parameter γ. A thorough investigation of the corresponding de Sitter and anti–de Sitter "backgrounds" in the form (9) (when n, γ, e, $g = 0$, with $\Lambda \neq 0$) was performed in Refs. [7,11]. The Minkowski "background" with $\Lambda = 0$, and the physical meaning of all seven independent parameters of Eq. (9), have been recently clarified in Ref. [8]. Clearly, by setting e, g, $\gamma = 0$, the class of metrics (9)–(10) reduces to the B metrics (8).

For both A and B metrics (4) and (8), the only nonzero Weyl curvature Newman-Penrose scalar is

$$\Psi_2 = \frac{n}{p^3} \tag{11}$$

(see Ref. [8]). The metrics are thus of algebraic type D (or conformally flat when $n = 0$) and have a curvature singularity at $p = 0$. Since the metrics depend on the fraction n/p, we may restrict ourselves to $p > 0$ while keeping n arbitrary. In order to keep the signature $(-, +, +, +)$, we must also constrain the range of p such that $\mathcal{P}(p) > 0$.

As noted already by Ehlers and Kundt in Ref. [1], the A metrics (4) and the B metrics (8) have very similar forms, formally related by a complex transformation $\varphi = \mathrm{i}t$ and $t = \mathrm{i}z$, implying $d\varphi^2 \to -dt^2$ and $dt^2 \to -dz^2$. However, this seems to be just a "heuristic trick," a specific kind of "Wick rotation." It is preferable to avoid such a formal identification. Instead, following Ref. [12], in Sec. II we will employ a different approach to relate the A and B metrics. This will be based on performing a *boost of the source*, a procedure more acceptable from the physical point of view. In Sec. III we will investigate the admitted coordinate ranges and possible extensions of the B metrics. Subsequently, in Sec. IV we will examine the main geometrical properties of the corresponding gravitational field of a tachyonic source, which can be composed of the AII and BI metrics, separated by the Mach-Cherenkov shocks. All these results will then be generalized to any value of the cosmological constant Λ in Secs. V–VII.

II. AII AND BI METRICS ARE THE SCHWARZSCHILD SPACETIME BOOSTED TO INFINITE SPEED

In 1970, Peres [12] realized that it is possible to obtain the exact gravitational field of a (hypothetical) tachyon by boosting the classic Schwarzschild source (written in

isotropic coordinates) to superluminal speed. In fact, by this procedure the Mach-Cherenkov shock wave is also generated which separates two distinct regions which are described by the *AII* and *BI* metrics. Such tachyonic counterparts of the Schwarzschild black hole solution were subsequently studied in more detail by Schulman [13] and Gott [14]. Let us first summarize this procedure by explicitly "boosting" the usual form of the Schwarzschild metric to infinite speed, obtaining thus

the gravitational field of a tachyon. Conversely, it is possible to "slow down" the tachyonic source of the *AII* and *BI* metrics to zero speed, obtaining thus the usual Schwarzschild *AI* metric of a static source. In this sense, the *AI*, *AII* and *BI* metrics are related and, in fact, "equivalent": they just represent (various regions of) the gravitational field generated by a massive source moving with all possible velocities, including zero and infinity.

A. Boosting the Schwarzschild (*AI*) metric to $v \to \infty$

The Schwarzschild metric in the form (4) with $\epsilon_2 = 1 = \epsilon_0$, $\Lambda = 0$, $n = -M$ can be written in Cartesian coordinates

$$p = r = \sqrt{X^2 + Y^2 + Z^2}, \qquad q = \cos\vartheta = \frac{Z}{\sqrt{X^2 + Y^2 + Z^2}}, \qquad \tan\varphi = \frac{Y}{X}, \qquad T = t, \tag{12}$$

as

$$ds^2 = -dT^2 + dX^2 + dY^2 + dZ^2 + \frac{2M}{\sqrt{X^2 + Y^2 + Z^2}}\left(dT^2 + \left(1 - \frac{2M}{\sqrt{X^2 + Y^2 + Z^2}}\right)^{-1}\frac{(XdX + YdY + ZdZ)^2}{X^2 + Y^2 + Z^2}\right). \tag{13}$$

Let us now perform a boost in the *Z* direction:

$$T = \frac{T' + vZ'}{\sqrt{1 - v^2}}, \qquad Z = \frac{Z' + vT'}{\sqrt{1 - v^2}}. \tag{14}$$

Although this boost is only allowed for velocities $|v| < 1$, it is interesting to observe that *all terms in the metric* (13) *that introduce* $\sqrt{1 - v^2}$ *via T and Z are quadratic*. It is thus possible to consider the limit $v \to \infty$, resulting in

$$\lim_{v\to\infty} T^2 = \lim_{v\to\infty} \frac{(T' + vZ')^2}{1 - v^2} = -Z'^2, \qquad \lim_{v\to\infty} Z^2 = \lim_{v\to\infty} \frac{(Z' + vT')^2}{1 - v^2} = -T'^2. \tag{15}$$

The "infinite boost" thus effectively causes *just a swap* $T^2 \to -Z'^2$ and $Z^2 \to -T'^2$, so that the exact Schwarzschild metric (13) becomes

$$ds^2 = -dT'^2 + dX^2 + dY^2 + dZ'^2 + \frac{2M}{\sqrt{-T'^2 + X^2 + Y^2}}\left(-dZ'^2 + \left(1 - \frac{2M}{\sqrt{-T'^2 + X^2 + Y^2}}\right)^{-1}\frac{(-T'dT' + XdX + YdY)^2}{-T'^2 + X^2 + Y^2}\right). \tag{16}$$

In fact, this is the *AII* metric in the region $T'^2 > X^2 + Y^2$ for *M* purely imaginary, and the *BI* metric in the complementary region $T'^2 < X^2 + Y^2$ for *M* real.

Indeed, the *AII* metric (4) with $\epsilon_2 = -1 = \epsilon_0$, $\Lambda = 0$, written in Cartesian coordinates

$$p = \sqrt{T^2 - X^2 - Y^2}, \qquad q = \frac{T}{\sqrt{T^2 - X^2 - Y^2}}, \qquad \tan\varphi = \frac{Y}{X}, \qquad t = Z, \tag{17}$$

reads

$$ds^2 = -dT^2 + dX^2 + dY^2 + dZ^2 + \frac{2n}{\sqrt{T^2 - X^2 - Y^2}}\left(-dZ^2 + \left(1 - \frac{2n}{\sqrt{T^2 - X^2 - Y^2}}\right)^{-1}\frac{(-TdT + XdX + YdY)^2}{-T^2 + X^2 + Y^2}\right). \tag{18}$$

This is exactly the boosted Schwarzschild metric (16) with the identification $M = in$, i.e., for purely imaginary mass of the (necessarily tachyonic) source. Here we consider the principal square root $\sqrt{-T'^2 + X^2 + Y^2} = i\sqrt{T'^2 - X^2 - Y^2}$. Of course, the transformation (17) is only valid in the region $T^2 > X^2 + Y^2$.

Similarly, the *BI* metric (8) with $\epsilon_2 = 1$, $\epsilon_0 = -1$ (which is a more convenient coordinate representation than $\epsilon_0 = 1$), $\Lambda = 0$ is put into Cartesian coordinates in the region $T^2 < X^2 + Y^2$ by

$$p = \sqrt{-T^2 + X^2 + Y^2}, \qquad q = \frac{T}{\sqrt{-T^2 + X^2 + Y^2}}, \qquad \tan t = \frac{Y}{X}, \quad z = Z, \tag{19}$$

taking the form

$$ds^2 = -dT^2 + dX^2 + dY^2 + dZ^2 - \frac{2n}{\sqrt{-T^2 + X^2 + Y^2}}\left(-dZ^2 + \left(1 + \frac{2n}{\sqrt{-T^2 + X^2 + Y^2}}\right)^{-1}\frac{(-TdT + XdX + YdY)^2}{-T^2 + X^2 + Y^2}\right). \tag{20}$$

Again, this is exactly the boosted Schwarzschild metric (16), in this case with $M = -n$.

B. Slowing the *AII* metric to $v \to 0$

Of course, it is also possible to consider a complementary procedure. Instead of boosting the Schwarzschild static source to infinite speed, we can stop the tachyonic source of the *AII* metric. This is achieved by performing the boost[2]

$$T = \frac{vT' - Z'}{\sqrt{v^2 - 1}}, \qquad Z = \frac{vZ' - T'}{\sqrt{v^2 - 1}} \tag{21}$$

of the metric (18). Although Eq. (21) is only allowed for $v > 1$, the metric is quadratic in T and Z, so it is possible to take the limit $v \to 0$, resulting in

$$\lim_{v \to 0} T^2 = \lim_{v \to 0}\frac{(vT' - Z')^2}{v^2 - 1} = -Z'^2, \qquad \lim_{v \to 0} Z^2 = \lim_{v \to 0}\frac{(vZ' - T')^2}{v^2 - 1} = -T'^2. \tag{22}$$

As in the case (15), the limit $v \to 0$ causes the swap $T^2 \to -Z'^2$ and $Z^2 \to -T'^2$. The *AII* metric (18), valid in $T^2 > X^2 + Y^2$, slowed down to $v = 0$ is thus

$$ds^2 = -dT'^2 + dX^2 + dY^2 + dZ'^2 + \frac{2n}{\sqrt{-X^2 - Y^2 - Z'^2}}\left(dT'^2 + \left(1 - \frac{2n}{\sqrt{-X^2 - Y^2 - Z'^2}}\right)^{-1}\frac{(XdX + YdY + Z'dZ')^2}{X^2 + Y^2 + Z'^2}\right). \tag{23}$$

In the region $X^2 + Y^2 + Z'^2 > 0$ this is the Schwarzschild metric (13) with $n = iM$.

C. Slowing the *BI* metric to $v \to 0$

Using the boost (21) we can similarly stop the superluminal tachyonic source of the *BI* metric. Due to the swap (22), the metric (20) valid in the region $T^2 < X^2 + Y^2$ becomes

$$ds^2 = -dT'^2 + dX^2 + dY^2 + dZ'^2 - \frac{2n}{\sqrt{X^2 + Y^2 + Z'^2}}\left(dT'^2 + \left(1 + \frac{2n}{\sqrt{X^2 + Y^2 + Z'^2}}\right)^{-1}\frac{(XdX + YdY + Z'dZ')^2}{X^2 + Y^2 + Z'^2}\right), \tag{24}$$

which is the Schwarzschild metric (13) in the region $X^2 + Y^2 + Z'^2 > 0$, just with the relabeling $M = -n$.

---

[2]This is formally the same as Eq. (14) with v replaced by $-1/v$.

Both the *AII* and *BI* metrics can thus be physically interpreted as (a formal limit of) the Schwarzschild solution boosted to an infinite speed. Conversely, the superluminal sources of the *AII* and *BI* metrics can be slowed down and even stopped, yielding exactly the classic Schwarzschild metric of a static massive source. In this sense, all three of these exact metrics can be understood as representing the "same gravitational field," with the *distinction given only by the speed of the source* and the *region* of spacetime covered by the corresponding coordinates.

It can also be seen that in the weak-field limit $n \to 0$, the "interior" *AII* metric (18) covering $T^2 > X^2 + Y^2$ and the "exterior" *BI* metric (20) covering $T^2 < X^2 + Y^2$ *together cover the whole Minkowski spacetime*, except the surface $T^2 = X^2 + Y^2$ between them. Physically, it identifies an expanding cylindrical *Mach-Cherenkov shock wave* which will be described in more detail in Sec. IV, and extended to any value of the cosmological constant Λ in Sec. VII.

III. COORDINATE RANGES OF THE B METRICS

It is now important to investigate the admitted coordinate ranges of the B metrics. We start with the case $\Lambda = 0$; more general B metrics with a cosmological constant Λ will be described in Sec. VI.

A. The BI metric

The *BI* metric is given by Eq. (8) with $\epsilon_2 = 1$, $\Lambda = 0$, that is

$$ds^2 = -p^2(\epsilon_0 - q^2)dt^2 + \frac{p^2}{\epsilon_0 - q^2}dq^2$$
$$+ \left(1 + \frac{2n}{p}\right)dz^2 + \left(1 + \frac{2n}{p}\right)^{-1}dp^2. \quad (25)$$

Here $z \in \mathbb{R}$, while the range of t, q depends on ϵ_0. Ehlers and Kundt in Ref. [1] considered the case $\epsilon_0 = 1$; see Table I. Due to Eq. (11), the range of p in Eq. (25) depends on the sign of n. For $n > 0$ it is $p \in (0, \infty)$, with a curvature singularity at $p = 0$, while for $n < 0$ it is $p \in (2|n|, \infty)$. Therefore, the two cases $n > 0$ and $n < 0$ represent two distinct spacetimes with different global structures. Ehlers and Kundt also suggested a possible analytic extension of the *BI* metric with $n < 0$ to *include* $p = 2|n|$ in the p coordinate. For the choice $\epsilon_0 = -1$, this is achieved by the transformation[3]

$$p = 2|n|/(1-\rho^2), \quad q = \sinh\tau, \quad z = 2n\zeta, \quad t = \varphi, \quad (26)$$

which puts the metric (25) into the form

---

[3]The original Ehlers and Kundt transformation for $\epsilon_0 = 1$ is $q = \cosh\tau \sin\varphi$, $\tanh t = \tanh\tau / \cos\varphi$.

$$ds^2 = 4n^2[(1 - \rho^2)^{-2}(-d\tau^2 + \cosh^2\tau d\varphi^2)$$
$$+ \rho^2 d\zeta^2 + 4(1 - \rho^2)^{-4}d\rho^2] \quad (27)$$

[see the metric (2–3.47) in Ref. [1]]. Although the term $\rho^2 d\zeta^2$ vanishes at $\rho = 0$, there is *no curvature singularity*. The coordinates (27) of the *BI* metric thus better illustrate the behavior of the spacetime. At $\rho = 0$, corresponding to $p = 2|n|$, the curvature (11) reaches its *maximal but finite value* (in fact, it is impossible to reach the curvature singularity located at $p = 0$). With $\rho \to 1$ the spacetime becomes asymptotically flat (since $p \to \infty$); see also the corresponding embedding diagram for fixed values of τ and ζ shown in the right part of Fig. 3. Let us finally remark that in a section with fixed values of τ and φ and very small values of ρ, the two-dimensional spatial metric is approximately $ds_2^2 \approx 16n^2[d\rho^2 + \rho^2[d(\zeta/2)]^2]$. For *angular* coordinate $\zeta \in [0, 4\pi)$, such a section would be flat and regular at $\rho = 0$ (see also page 58 of Ref. [14]). However, as will be seen below, a natural interpretation of the coordinate ζ is that it is a *noncompact* coordinate (along an infinite z axis of cylinders) with the full range $\zeta \in \mathbb{R}$.

B. The BII metric

Analogously, it is possible to study the *BII* metrics. In particular, the metric (8) with $\Lambda = 0$, $\epsilon_2 = -1$ and $\epsilon_0 = 1$ (to avoid superficial coordinate singularities in q) is

$$ds^2 = -p^2(1 + q^2)dt^2 + \frac{p^2}{1 + q^2}dq^2$$
$$+ \left(\frac{2n}{p} - 1\right)dz^2 + \left(\frac{2n}{p} - 1\right)^{-1}dp^2. \quad (28)$$

The allowed ranges of coordinates are t, q, $z \in \mathbb{R}$, $p \in (0, 2n)$. The correct signature requires $n > 0$, and the metric (28) *does not admit the flat (Minkowski) limit* given by $n \to 0$. Similarly to Eq. (26) we may apply the transformation

$$p = 2n/(1 + \rho^2), \quad q = \sinh z, \quad z = 2n\zeta, \quad (29)$$

so that the *BII* metric (28) becomes

$$ds^2 = 4n^2[(1 + \rho^2)^{-2}(dz^2 - \cosh^2 z dt^2)$$
$$+ \rho^2 d\zeta^2 + 4(1 + \rho^2)^{-4}d\rho^2], \quad (30)$$

[see the metric (2–3.48) in Ref. [1]]. Again, there is no curvature singularity at $\rho = 0$ corresponding to $p = 2n$, while the curvature singularity at $p = 0$ corresponds to $\rho = \infty$.

C. The $BIII$ metric

This is obtained from Eq. (8) by setting $\epsilon_2 = 0$, $\epsilon_0 = 1$, $\Lambda = 0$,
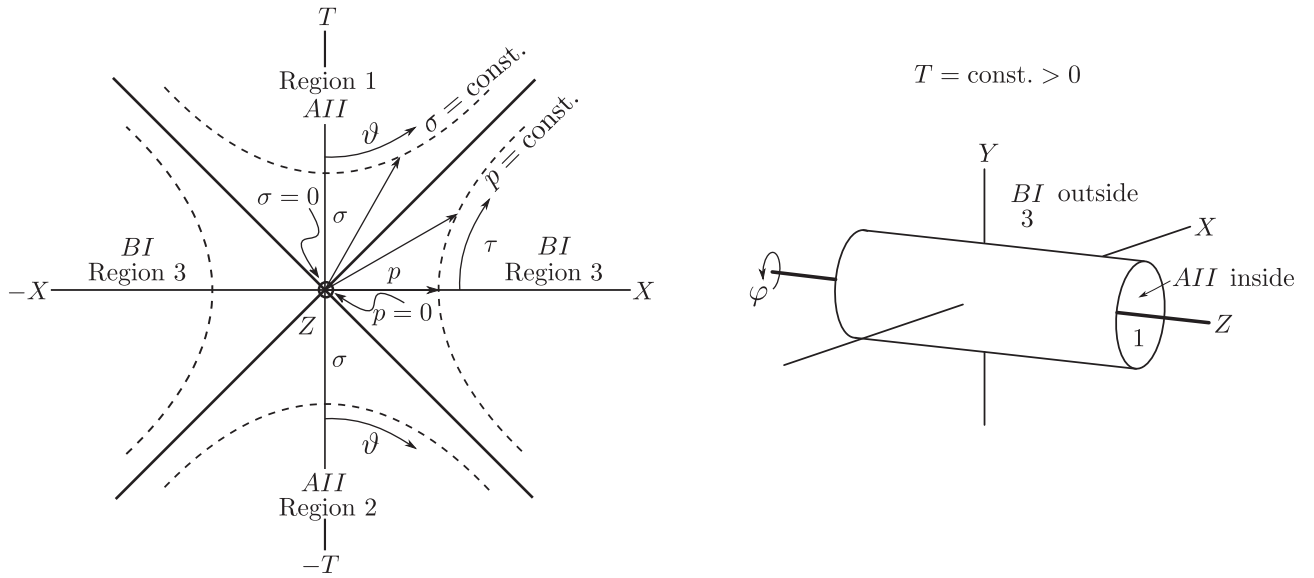
FIG. 1.   Complete Minkowski spacetime divided into Regions 1 and 2 covered by two "background" *AII* metrics (Region 1 for $T > 0$ and Region 2 for $T < 0$) and Region 3 covered by the "background" *BI* metric. The left part is the $T - X$ section with $Y = 0$ and Z arbitrary, while the right part shows the X, Y, Z subspace with $T = \text{const} > 0$. For $T > 0$ the boundary is an expanding cylinder whose interior is Region 1, while for $T < 0$ it is a contracting cylinder whose interior is Region 2. Outside this cylinder lies Region 3 covered by the *BI* metric. The tachyon moves along the Z axis with infinite speed.

$$ds^2 = -p^2 dt^2 + p^2 dq^2 + \frac{2n}{p} dz^2 + \frac{p}{2n} dp^2, \quad (31)$$

where $t, q, z \in \mathbb{R}$, $p \in (0, \infty)$. Necessarily $n > 0$, and the metric again does not have the Minkowski limit since $n = 0$ is prohibited. As argued in Refs. [4,8], it is a special Levi-Civita solution.

IV. GLOBAL STRUCTURE AND PHYSICAL INTERPRETATION

After establishing that both the *AII* metric and the *BI* metric represent specific parts of the gravitational field generated by a superluminal source (tachyon moving along a spacelike trajectory), it is now necessary to analyze the global structure of such spacetimes and their relation. In particular, we must describe the way in which the *AII* metric

$$ds^2 = \sigma^2 (d\vartheta^2 + \sinh^2\vartheta d\varphi^2)$$
$$+ \left(1 - \frac{2M}{\sigma}\right) dz^2 - \left(1 - \frac{2M}{\sigma}\right)^{-1} d\sigma^2, \quad (32)$$

[which is actually the *AII* metric (4) with $\epsilon_2 = -1 = \epsilon_0$, $n = M > 0$, $\Lambda = 0$, using $p = \sigma > 0$, $q = \cosh\vartheta$ and $t = z$] is *combined* with the *BI* metric

$$ds^2 = p^2(-d\tau^2 + \cosh^2\tau d\varphi^2)$$
$$+ \left(1 - \frac{2M}{p}\right) dz^2 + \left(1 - \frac{2M}{p}\right)^{-1} dp^2, \quad (33)$$

[which is the *BI* metric (8) with $\epsilon_2 = 1$, $\epsilon_0 = -1$, $n = -M < 0$, $\Lambda = 0$, using $q = \sinh\tau$, $t = \varphi$].

A. Weak-field limit

As suggested already by Gott [14], in the weak-field limit $M \to 0$ the curved spacetime around the tachyonic source becomes flat Minkowski spacetime, with the tachyon becoming just a *test particle located along the Z axis* (identical to the z axis). The flat spacetime is *divided into distinct regions that are separated by the cylindrical surface* $T^2 = X^2 + Y^2$ with Z arbitrary, as shown in Fig. 1.

Region 1 and Region 2 are given by $T^2 > X^2 + Y^2$ with $T > 0$ and $T < 0$, respectively. These are covered by the metric (32) with $M = 0$, namely

$$ds^2 = \sigma^2(d\vartheta^2 + \sinh^2\vartheta d\varphi^2) + dz^2 - d\sigma^2, \quad (34)$$

whose coordinates are related to background Minkowski coordinates as $Z = z$,

$$T = \pm\sigma \cosh\vartheta,$$
$$X = \sigma \sinh\vartheta \cos\varphi,$$
$$Y = \sigma \sinh\vartheta \sin\varphi, \quad (35)$$

so that $T^2 - X^2 - Y^2 = \sigma^2$. Any $\sigma = \text{const}$ is thus a hyperboloidal surface. Notice however that the coordinate singularity $\sigma = 0$ actually corresponds to

$$T = 0, \qquad X = 0 = Y, \quad (36)$$

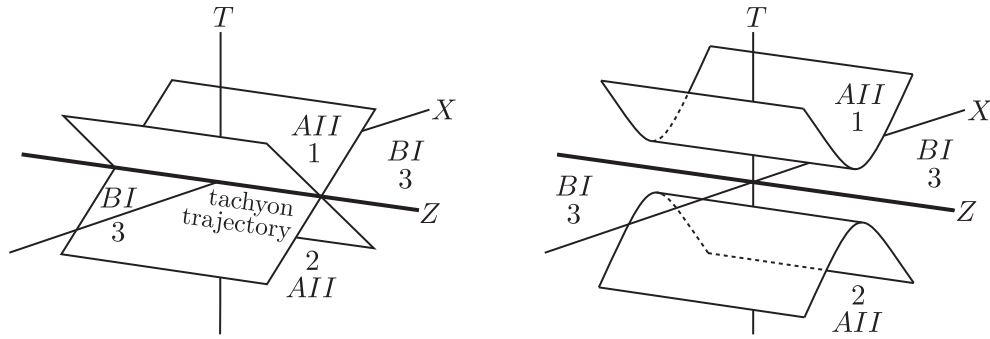which is just the Z axis, i.e., *the tachyon trajectory*.

FIG. 2.   The T, X, Z subspace of Minkowski spacetime for $Y = 0$ (left) and for a constant $Y \neq 0$ (right). It is divided into the two disconnected Regions 1 and 2 with the AII metrics, and Region 3 with the BI metric.

Region 3 is defined by $T^2 < X^2 + Y^2$. It is covered by the flat limit of the BI metric (33)

$$ds^2 = p^2(-d\tau^2 + \cosh^2\tau d\varphi^2) + dz^2 + dp^2, \quad (37)$$

corresponding to Minkowski coordinates via $Z = z$,

$$T = p \sinh \tau,$$
$$X = p \cosh \tau \cos \varphi,$$
$$Y = p \cosh \tau \sin \varphi, \quad (38)$$

so that $X^2 + Y^2 - T^2 = p^2$. Therefore, $p = \text{const}$ is a hyperboloidal surface, but the coordinate singularity $p = 0$ again corresponds to the line $T = 0$, $X = 0 = Y$, i.e., it is the tachyon trajectory along the Z axis. It is now also clear that both regions $X > 0$ and $X < 0$ are covered by taking the full range of the angular coordinate $\varphi \in [0, 2\pi)$. Moreover, Region 1 for $Y \neq 0$ is explicitly disconnected from Region 2; see Fig. 2. Thus, two copies of the metric (34) together with the single metric (37) cover the whole Minkowski space (except the separation boundary $X^2 + Y^2 = T^2$), as shown in Figs. 1 and 2.

B. Curved metrics and their analytic extension

Of course, with $M \neq 0$ the complete spacetime covered by pairs of Eqs. (32) and (33) is not flat anymore. In fact, there is a "tachyonic-type" *curvature singularity* located at $\sigma = 0$ for the AII metric, and formally at $p = 0$ for the BI metric; see Eq. (11).

Despite the presence of such a curvature singularity, both of the metrics *remain asymptotically flat far away from the tachyonic source*, i.e., for large σ and p. Indeed, by inspecting the Cartesian form of the AII metric (18) it can be observed that for *any finite* X, Y, Z, the metric becomes $ds^2 \approx -dT^2 + dX^2 + dY^2 + dZ^2$ as $|T| \to \infty$. The same is true for the BI metric (20) for *any finite* T and $X^2 + Y^2 \to \infty$.

There is a coordinate singularity in the AII metric (32) at $\sigma = 2M > 0$. This is clearly the *Killing horizon* generated by the Killing vector ∂_z. For $\sigma > 2M$ the coordinate z is spatial, and in this region the metric is time dependent (σ is

a temporal coordinate). On the other hand, for $0 < \sigma < 2M$ the coordinate z is temporal, and the spacetime region is static (σ is a spatial coordinate). The AII metric can be maximally analytically extended across $\sigma = 2M$; see Ref. [14] and Sec. 9.1.1 of Ref. [4] for more details. The corresponding Penrose conformal diagram can be constructed by employing the Kruskal–Szekeres-type coordinates. This is shown in the left part of Fig. 3, and illustrates the null character of the horizons $\sigma = 2M$, the timelike character of the curvature singularities $\sigma = 0$, and asymptotically flat null infinities $\mathcal{I}^\pm$ at $\sigma = \infty$.

Similarly, the BI metric (33) with $M \neq 0$ ceases to be flat, covering the background exterior region $T^2 < X^2 + Y^2$ via Eq. (38). There is a curvature singularity at $p = 0$. However,

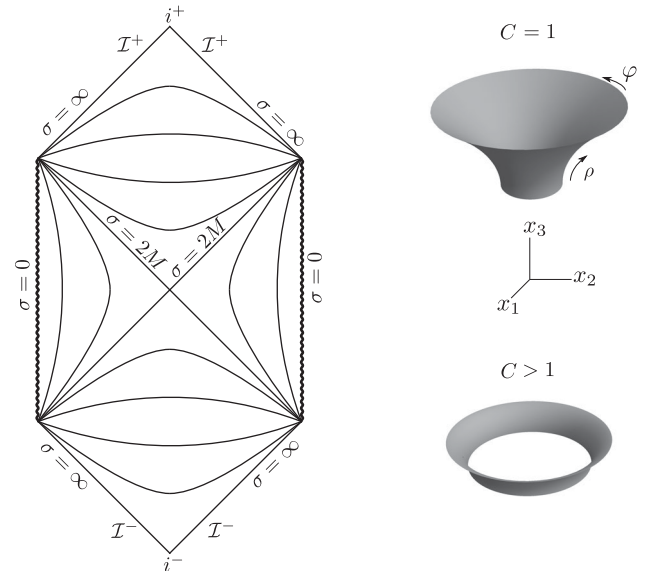FIG. 3.   Left: Global conformal diagram for the AII metric (32) with coordinates ϑ, φ suppressed (in particular, $\vartheta = 0$). Here $i^\pm$ denote past/future timelike infinities, while $\mathcal{I}^\pm$ are null conformal infinities. The horizons $\sigma = 2M$ are null, while the singularities $\sigma = 0$ are timelike. Right: Embedding diagram of the BI metric (40) for the section $z = \text{const}$ and $\cosh \tau \equiv C = \text{const}$. For larger C, the neck diameter grows, while the surface becomes more restricted.

as explained in Sec. III A, this singularity *cannot be reached* because only the range $p \in (2M, \infty)$ is allowed. The *BI* metric can be extended to include $p = 2M > 0$ by performing the transformation $p = 2M/(1 - \rho^2)$ and taking $\rho \in [0, 1)$, so that the metric becomes

$$ds^2 = 4M^2(1 - \rho^2)^{-4}[(1 - \rho^2)^2(-d\tau^2 + \cosh^2\tau d\varphi^2) + 4d\rho^2] + \rho^2 dz^2, \tag{39}$$

cf. Eqs. (26) and (27). On the boundary $\rho = 0$, corresponding to $p = 2M$, the curvature (11) is maximal but finite. Its geometry is $ds_2^2 = 4M^2(-d\tau^2 + \cosh^2\tau d\varphi^2)$ which is a two-dimensional de Sitter space.

For any fixed values of τ and z, the extended *BI* metric (39) reads

$$ds_2^2 = 4M^2(1 - \rho^2)^{-4}[4d\rho^2 + (1 - \rho^2)^2 C^2 d\varphi^2], \tag{40}$$

where $C \equiv \cosh\tau \geq 1$ is a constant. *This geometry can be embedded* into three-dimensional Euclidean space with Cartesian coordinates by

$$x_1 = \frac{2MC}{1 - \rho^2}\cos\varphi, \qquad x_2 = \frac{2MC}{1 - \rho^2}\sin\varphi,$$

$$x_3 = 4M \int \frac{\sqrt{1 - C^2\rho^2}}{(1 - \rho^2)^2} d\rho. \tag{41}$$

For $\tau = 0$, corresponding to $C = 1$, we explicitly obtain $x_3 = 4M\rho/\sqrt{1 - \rho^2}$. The embedding surface $x_3^2 = 8M \times (\sqrt{x_1^2 + x_2^2} - 2M)$, shown in the upper right part of Fig. 3, extends to infinite values of x_i because the whole range $\rho \in [0, 1)$ is allowed. For $C > 1$ the integral in Eq. (41) is more complicated. Numerical integration leads to the axially symmetric embedding surface shown in the lower right part of Fig. 3. As $\tau > 0$ (and thus C) grows, the radius

$2MC$ of the neck at $\rho = 0$ grows, while the allowed range of ρ in Eq. (41) becomes more restricted to $\rho < 1/C$.

C. Mach-Cherenkov shock wave separating the *AII* and *BI* metrics

It has been demonstrated in Sec. IV A that, in the weak-field limit $M \to 0$, the complete Minkowski spacetime is covered by two "background" *AII* metrics (Regions 1 and 2 for $T > 0$ and $T < 0$, respectively) and one "background" *BI* metric (Region 3). These are separated by the *cylindrical surface* $X^2 + Y^2 = T^2$ with Z arbitrary; see Fig. 1. This cylinder *contracts* for $T < 0$ to the Z axis located at $T = 0$, which is just the tachyon trajectory, and then *reexpands* for $T > 0$. The spacetime region inside this cylinder is covered by the *AII* metric, while its exterior is covered by the *BI* metric. The cylindrical boundary between them, which contracts/expands at the speed of light to/from the tachyon trajectory, is the *Mach-Cherenkov shock wave generated by the superluminal source*. Since the tachyon moves with *infinite speed*, the "Mach-Cherenkov cone" is "infinitely sharp," i.e., it has a cylindrical geometry.

Of course, with $M \neq 0$ the distinct regions covered by the *AII* and *BI* metrics *cannot be joined smoothly* across the Mach-Cherenkov surface. While *keeping the cylindrical geometry*, it becomes a surface with a *discontinuity* because the specific curvatures on both of its sides are different. This gives rise to a *real gravitational shock wave*, whose jump in the curvature can be explicitly evaluated. Instead of using the coordinate representations (32) and (33), this can be explicitly performed in the Cartesian coordinates. Notice that the cylindrical surface $X^2 + Y^2 = T^2$, Z arbitrary, formally degenerates to $\sigma = 0$, $\vartheta = \infty$ in Eq. (34) and $p = 0$, $\tau = \infty$ in Eq. (37). By combining the *AII* and *BI* metrics in the Cartesian coordinates (18) and (20), it is possible to write a *unified metric for both parts of the curved spacetime* in the whole range of the background coordinates T, X, Y, Z as

$$ds^2 = -dT^2 + dX^2 + dY^2 + dZ^2 + \frac{2M}{\sqrt{|T^2 - X^2 - Y^2|}}\left(-dZ^2 + \left(1 - \frac{2M}{\sqrt{|T^2 - X^2 - Y^2|}}\right)^{-1}\frac{(-TdT + XdX + YdY)^2}{-T^2 + X^2 + Y^2}\right). \tag{42}$$

For $T^2 > X^2 + Y^2$ this is the *AII* metric (18) with $M \equiv n$, while for $T^2 < X^2 + Y^2$ this is the *BI* metric (20) with $M \equiv -n$.[4] The metric (42) diverges on the shock surface $X^2 + Y^2 = T^2$. In fact, there is an *infinite discontinuity in the Weyl curvature scalar* Ψ_2 [Eq. (11)], namely

$$\Psi_2 = +M(T^2 - X^2 - Y^2)^{-3/2} \quad \text{for } T^2 > X^2 + Y^2,$$
$$\Psi_2 = -M(-T^2 + X^2 + Y^2)^{-3/2} \quad \text{for } T^2 < X^2 + Y^2. \tag{43}$$

The curvature singularity located at the Mach-Cherenkov cylindrical shock wave is such that $\Psi_2 \to +\infty$ when it is approached from its interior, while $\Psi_2 \to -\infty$ when it is approached from its exterior.

D. Boosted metrics

In order to better understand and illustrate the tachyon motion and also the specific character of the generated

---

[4]It is natural to choose $M = -n$ to obtain the *same* parameter $M > 0$ for both parts of the unified metric (42). The alternative choice $M = n$ for the *BI* metric is mathematically also possible. In such a case the curvature scalar would behave as $\Psi_2 = M|T^2 - X^2 - Y^2|^{-3/2}$, but the metric on both parts would look different.
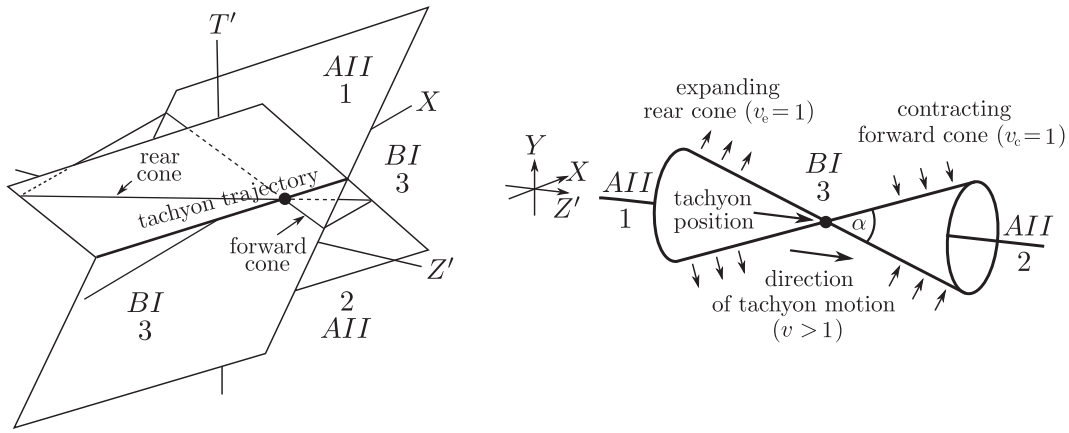
FIG. 4.   Minkowski spacetime separated into Regions 1, 2, and 3 by the Mach-Cherenkov shock cones generated by the tachyon slowed down by a boost to finite superluminal speed. The spacetime structure is visualized in the sections $Y = 0$ (left) and $T' = $ const > 0 (right). The tachyon moves in the Z' direction, and generates an expanding rear cone and contracting forward cone.

Mach-Cherenkov cone, it is very convenient to consider a boost of the metric, as originally suggested in Ref. [14].

Since the tachyonic source in Eqs. (34) and (37), and also Eqs. (32) and (33), moves at *infinite speed* (it is instantaneously located everywhere along on the Z axis), such a boost will actually *slow it down to finite* superluminal speed $v > 1$. We will use the boost (21). The boosted tachyon then moves in the Z' direction (coinciding with z') at the speed $v > 1$. In the new coordinates, the surface $\sqrt{X^2 + Y^2} = T$ that separates Regions 1 and 3, and the surface $\sqrt{X^2 + Y^2} = -T$ that separates Regions 2 and 3, take the form

$$X^2 + Y^2 = \frac{(vT' - Z')^2}{v^2 - 1}. \tag{44}$$

At any fixed time T', these represent *Mach-Cherenkov shock cones* with the vertex at $Z' = vT'$ which is the *actual position of the tachyon*, and with the *angle* α of the cone such that $\alpha = 2 \operatorname{arccot}\sqrt{v^2 - 1}$. As illustrated in Fig. 4, the *rear cone expands* while the *forward cone contracts* at the speed of light. The tachyon is always located at the intersection of these cones and—in a manner similar to the so-called scissors effect—moves faster than light.

It is also illustrative to plot these shock waves for *different speeds* $v > 1$ of the tachyon; see Fig. 5. For larger superluminal v, the angle α of the cone is smaller. In the extreme case $v = \infty$ this angle is zero and the cone degenerates to the cylinder plotted in Fig. 1, while in the opposite limit $v = 1$ both the rear and front cones degenerate to the point $X = 0 = Y$ moving at the speed of light in the Z' direction, which is the position of the tachyon. This behavior follows from the dependence of the regions on v. The interior Regions 1 and 2 covered by two separate AII metrics are located at $X^2 + Y^2 < (vT' - Z')^2/(v^2 - 1)$, so that *for smaller superluminal speed* v these regions are *larger*. In the limit $v \to 1$ the whole spacetime (except the surface $Z' = T'$) is covered

by the pair of AII metrics. On the other hand, Region 3 defined by $X^2 + Y^2 > (vT' - Z')^2/(v^2 - 1)$ becomes *smaller*, and in the limit $v \to 1$ it degenerates to the surface $Z' = T'$ except for the line $X = 0 = Y$. The surface that separated Regions 1, 2 and 3 degenerates to a line $Z' = T'$, $X = 0 = Y$ (worldline of the tachyon).

V. AII AND BI METRICS WITH Λ ARE THE SCHWARZSCHILD–(ANTI–)DE SITTER SPACETIME BOOSTED TO INFINITE SPEED

In previous sections we considered the A and B metrics in a Minkowski background by setting $\Lambda = 0$ in the metrics (4) and (8), respectively. Now we are going to extend the results to any value of the cosmological constant. In fact, we will demonstrate that these metrics can be understood as specific regions of the spacetime representing the exact gravitational field of a tachyonic source moving in a de Sitter (if $\Lambda > 0$) or anti–de Sitter (if $\Lambda < 0$) universe.

First, let us investigate boosts of the classic Schwarzschild–(anti–)de Sitter metric (which is the most important AI metric with Λ) and perform the limit $v \to \infty$. However, with $\Lambda \neq 0$ the background is not flat but it is everywhere curved (anti–)de Sitter spacetime. To perform the boost correctly, it is most convenient to employ a five-dimensional embedding formalism. It is well known that (anti–)de Sitter spacetime can be understood as a hyperboloid

$$-Z_0^2 + Z_1^2 + Z_2^2 + Z_3^2 + \epsilon Z_4^2 = \epsilon a^2, \tag{45}$$

embedded into a five-dimensional flat spacetime

$$\mathrm{d}s^2 = -\mathrm{d}Z_0^2 + \mathrm{d}Z_1^2 + \mathrm{d}Z_2^2 + \mathrm{d}Z_3^2 + \epsilon \mathrm{d}Z_4^2, \tag{46}$$

where $a \equiv \sqrt{3/|\Lambda|}$ and $\epsilon \equiv \operatorname{sign} \Lambda$; see the visualizations in Fig. 6.
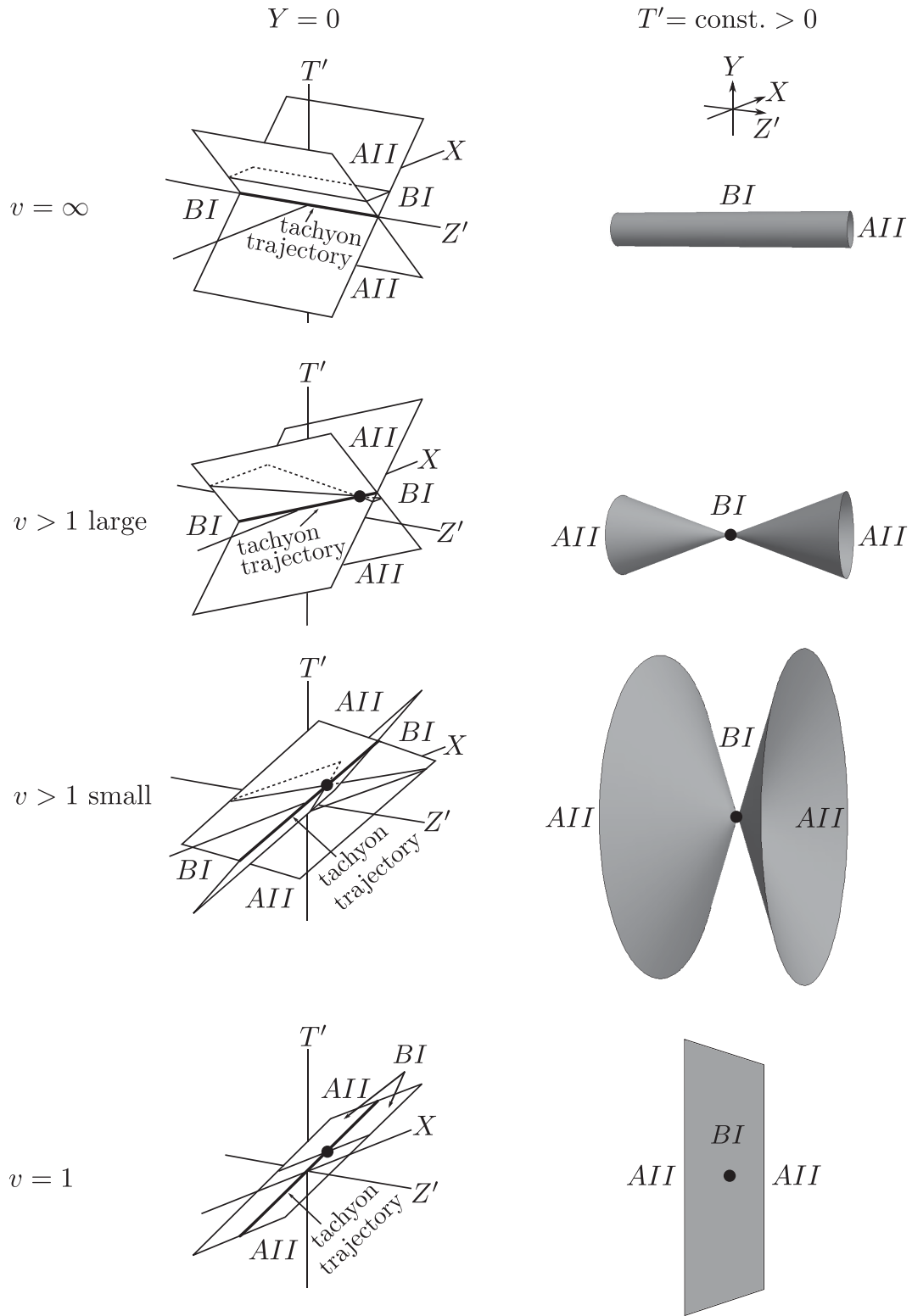
FIG. 5.   The spacetime structure (left), consisting of the *AII* and *BI* metrics separated by the Mach-Cherenkov shock waves (right) for various superluminal speeds v of the tachyonic source.
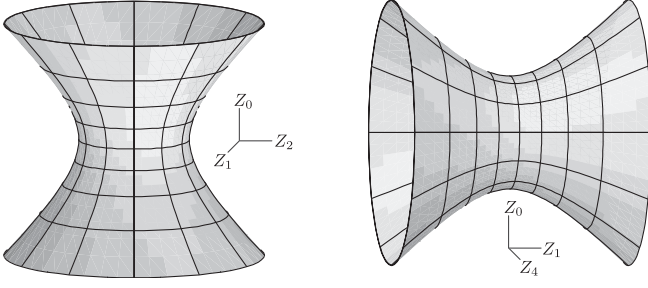
FIG. 6.   The visualizations of de Sitter spacetime (left) and anti–de Sitter spacetime (right) as hyperboloids (45) embedded in a flat five-dimensional spacetime (46). The remaining coordinates (Z_3, Z_4 for $\Lambda > 0$, and Z_2, Z_3 for $\Lambda < 0$) are suppressed. For more details see Ref. [4].

The (anti–)de Sitter background is obtained from the AI metric (4) for $\epsilon_2 = 1 = \epsilon_0$, $n = 0$. In the case with $\Lambda > 0$, these coordinates parametrize the hyperboloid (45) as

$$
\left.
\begin{aligned}
Z_0 &= \pm\sqrt{a^2 - p^2}\,\sinh(t/a), \\
Z_1 &= p\sqrt{1 - q^2}\,\cos\varphi, \\
Z_2 &= p\sqrt{1 - q^2}\,\sin\varphi, \\
Z_3 &= pq, \\
Z_4 &= \pm\sqrt{a^2 - p^2}\,\cosh(t/a),
\end{aligned}
\right\} \quad \text{for } p < a,
$$

$$
\left.
\begin{aligned}
Z_0 &= \pm\sqrt{p^2 - a^2}\,\cosh(t/a), \\
Z_1 &= p\sqrt{1 - q^2}\,\cos\varphi, \\
Z_2 &= p\sqrt{1 - q^2}\,\sin\varphi, \\
Z_3 &= pq, \\
Z_4 &= \pm\sqrt{p^2 - a^2}\,\sinh(t/a),
\end{aligned}
\right\} \quad \text{for } p > a, \qquad (47)
$$

while for $\Lambda < 0$ the corresponding parametrization is

$$
\begin{aligned}
Z_0 &= \sqrt{a^2 + p^2}\,\sin(t/a), \\
Z_1 &= p\sqrt{1 - q^2}\,\cos\varphi, \\
Z_2 &= p\sqrt{1 - q^2}\,\sin\varphi, \\
Z_3 &= pq, \\
Z_4 &= \sqrt{a^2 + p^2}\,\cos(t/a).
\end{aligned} \qquad (48)
$$

Expressing the AI metric (4) with $\epsilon_2 = 1 = \epsilon_0$ and $n \neq 0$ in these five-dimensional coordinates, using Eqs. (47) and (48), we obtain

$$
ds^2 = ds^2_{(A)dS} + \frac{2Ma^2}{p}\left(\frac{(Z_4 dZ_0 - Z_0 dZ_4)^2}{(Z_4^2 - \epsilon Z_0^2)^2}\right.
$$
$$
\left. + \frac{a^2}{p^2}\frac{(Z_0 dZ_0 - \epsilon Z_4 dZ_4)^2}{(Z_4^2 - \epsilon Z_0^2)(Z_4^2 - \epsilon Z_0^2 - 2Ma^2/p)}\right), \qquad (49)
$$

where $ds^2_{(A)dS}$ is the (anti–)de Sitter background metric (46), $M \equiv -n$ and $p = \sqrt{Z_1^2 + Z_2^2 + Z_3^2}$. As in Refs. [15–17], we can make a boost similar to Eq. (14), but now in the coordinates Z_0, Z_3:

$$
Z_0 = \frac{Z_0' + vZ_3'}{\sqrt{1 - v^2}}, \qquad Z_3 = \frac{Z_3' + vZ_0'}{\sqrt{1 - v^2}}. \qquad (50)
$$

We immediately observe that all the terms introducing the factor $\sqrt{1 - v^2}$ into Eq. (49) are *quadratic*, so it is possible to take the formal limit $v \to \infty$ that will effectively cause just a swap $Z_0^2 \to -Z_3'^2$ and $Z_3^2 \to -Z_0'^2$ in Eq. (49). The resulting metric will thus become

$$
ds^2 = ds^2_{(A)dS} + \frac{2Ma^2}{p}\left(\frac{-(Z_4 dZ_3' - Z_3' dZ_4)^2}{(Z_4^2 + \epsilon Z_3'^2)^2}\right.
$$
$$
\left. + \frac{a^2}{p^2}\frac{(Z_3' dZ_3' + \epsilon Z_4 dZ_4)^2}{(Z_4^2 + \epsilon Z_3'^2)(Z_4^2 + \epsilon Z_3'^2 - 2Ma^2/p)}\right), \qquad (51)
$$

where $p = \sqrt{Z_1^2 + Z_2^2 - Z_0'^2}$. This is the AII metric in the region $Z_0'^2 > Z_1^2 + Z_2^2$ with a purely imaginary mass, and the BI metric in the region $Z_0'^2 < Z_1^2 + Z_2^2$ with a real mass.

Indeed, the AII metric background (4) for $\epsilon_2 = -1 = \epsilon_0$, $n = 0$, with $\Lambda > 0$ is given by

$$
\begin{aligned}
Z_0 &= pq, \\
Z_1 &= p\sqrt{q^2 - 1}\,\cos\varphi, \\
Z_2 &= p\sqrt{q^2 - 1}\,\sin\varphi, \\
Z_3 &= \sqrt{p^2 + a^2}\,\cos(t/a), \\
Z_4 &= \sqrt{p^2 + a^2}\,\sin(t/a),
\end{aligned} \qquad (52)
$$

and with $\Lambda < 0$

$$
\left.
\begin{aligned}
Z_0 &= pq, \\
Z_1 &= p\sqrt{q^2 - 1}\,\cos\varphi, \\
Z_2 &= p\sqrt{q^2 - 1}\,\sin\varphi, \\
Z_3 &= \pm\sqrt{a^2 - p^2}\,\sinh(t/a), \\
Z_4 &= \pm\sqrt{a^2 - p^2}\,\cosh(t/a),
\end{aligned}
\right\} \quad \text{for } p < a,
$$

$$
\left.
\begin{aligned}
Z_0 &= pq, \\
Z_1 &= p\sqrt{q^2 - 1}\,\cos\varphi, \\
Z_2 &= p\sqrt{q^2 - 1}\,\sin\varphi, \\
Z_3 &= \pm\sqrt{p^2 - a^2}\,\cosh(t/a), \\
Z_4 &= \pm\sqrt{p^2 - a^2}\,\sinh(t/a),
\end{aligned}
\right\} \quad \text{for } p > a. \qquad (53)
$$

These parametrizations only cover the region $Z_0^2 > Z_1^2 + Z_2^2$. The complete AII metric with $n \neq 0$ written in the coordinates of Eqs. (52) and (53) thus has the form

$$ds^2 = ds^2_{(A)dS} + \frac{2na^2}{p}\left(\frac{-(Z_4 dZ_3 - Z_3 dZ_4)^2}{(Z_4^2 + \epsilon Z_3^2)^2}\right.$$
$$\left. - \frac{a^2}{p^2}\frac{(Z_3 dZ_3 + \epsilon Z_4 dZ_4)^2}{(Z_4^2 + \epsilon Z_3^2)(Z_4^2 + \epsilon Z_3^2 - 2na^2/p)}\right), \quad (54)$$

where $p = \sqrt{Z_0^2 - Z_1^2 - Z_2^2}$. We clearly see that this is exactly the Schwarzschild–(anti–)de Sitter metric (51) boosted to infinite speed, with the identification $M = \mathrm{i}n$ (and $p^2 \to -p^2$).

Similarly, the *BI* metric (8) for $\epsilon_2 = 1$, $\epsilon_0 = -1$, $n = 0$ corresponds to the parametrization

$$\left.\begin{aligned}
Z_0 &= pq, \\
Z_1 &= p\sqrt{1+q^2}\cos t, \\
Z_2 &= p\sqrt{1+q^2}\sin t, \\
Z_3 &= \sqrt{a^2 - p^2}\cos(z/a), \\
Z_4 &= \sqrt{a^2 - p^2}\sin(z/a),
\end{aligned}\right\} \quad \text{for } \Lambda > 0,$$

$$\left.\begin{aligned}
Z_0 &= pq, \\
Z_1 &= p\sqrt{1+q^2}\cos t, \\
Z_2 &= p\sqrt{1+q^2}\sin t, \\
Z_3 &= \pm\sqrt{a^2 + p^2}\sinh(z/a), \\
Z_4 &= \pm\sqrt{a^2 + p^2}\cosh(z/a),
\end{aligned}\right\} \quad \text{for } \Lambda < 0, \quad (55)$$

which only covers the region $Z_0^2 < Z_1^2 + Z_2^2$. In terms of the coordinates (55), the complete *BI* metric reads

$$ds^2 = ds^2_{(A)dS} + \frac{2na^2}{p}\left(\frac{(Z_4 dZ_3' - Z_3' dZ_4)^2}{(Z_4^2 + \epsilon Z_3'^2)^2}\right.$$
$$\left. - \frac{a^2}{p^2}\frac{(Z_3' dZ_3' + \epsilon Z_4 dZ_4)^2}{(Z_4^2 + \epsilon Z_3'^2)(Z_4^2 + \epsilon Z_3'^2 + 2na^2/p)}\right), \quad (56)$$

which is again the same as the Schwarzschild–de Sitter metric boosted to infinite speed [Eq. (51)] with $M = -n$ and $p = \sqrt{Z_1^2 + Z_2^2 - Z_0^2}$.

We may thus conclude that *both* the *AII* and *BI* metrics with any Λ can be understood as (formal) *limits of the classic Schwarzschild–(anti–)de Sitter metric boosted to infinite speed*. Of course, complementary procedures can also be applied: the Schwarzschild–de Sitter metric can be obtained by slowing down (stopping) the source of the *AII* metric with imaginary mass, or the *BI* metric with real mass.

VI. COORDINATE RANGES OF THE *B* METRICS WITH $\Lambda \neq 0$

To understand the global character of the *B* metrics with any cosmological constant, and their possible extensions and combinations, it is necessary to analyze the admitted coordinate ranges.

A. *BI* metric with Λ

For $\epsilon_2 = 1$ the metric (8) is

$$ds^2 = -p^2(\epsilon_0 - q^2)dt^2 + \frac{p^2}{\epsilon_0 - q^2}dq^2$$
$$+ \left(1 + \frac{2n}{p} - \frac{\Lambda}{3}p^2\right)dz^2 + \left(1 + \frac{2n}{p} - \frac{\Lambda}{3}p^2\right)^{-1}dp^2. \quad (57)$$
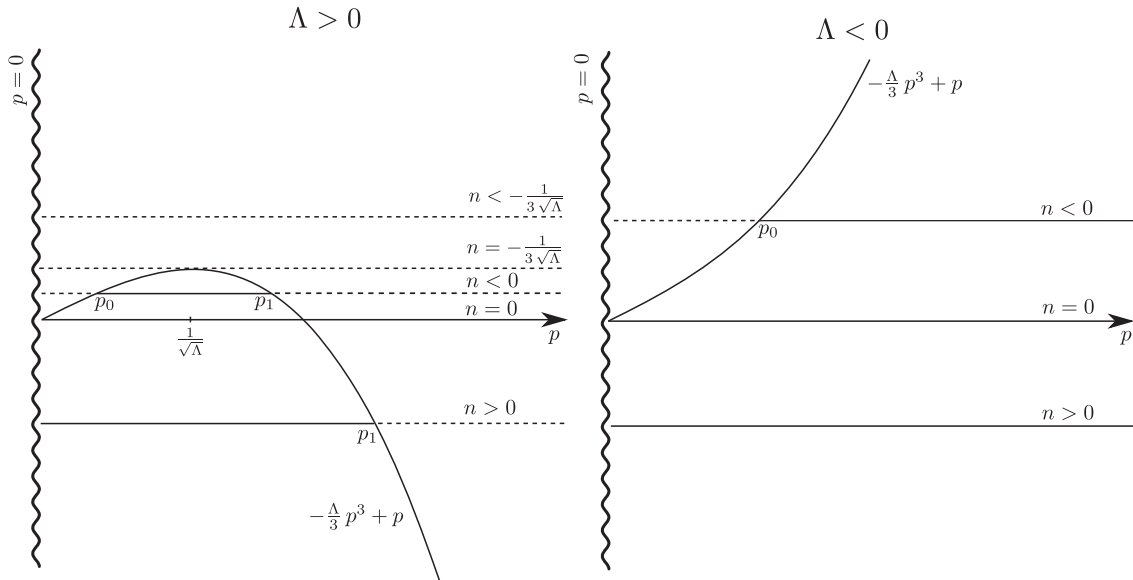

FIG. 7.   Allowed ranges of the coordinate p for $\Lambda > 0$ (left) and $\Lambda < 0$ (right) in the *BI* metric (57). The horizontal lines correspond to different values of $-2n$. The parts of these lines that lie under the curve $-\frac{\Lambda}{3}p^3 + p$ determine the admitted range of p. Their parts above the curve are dashed: there is no solution for these values because the metric would no longer have the correct signature. The intersections mark the roots p_0, p_1 of Eq. (58), with $0 < p_0 < p_1$.

The coordinate ranges are (considering $\epsilon_0 = -1$) $q, z \in \mathbb{R}$, $t \in [0, 2\pi)$, while the range of p depends on n and Λ. It is determined by the roots of the cubic equation

$$-\frac{\Lambda}{3} p^3 + p + 2n = 0. \tag{58}$$

The best way to illustrate the allowed ranges of $p > 0$ for all possible cases is to plot the possible roots p_i of Eq. (58) as intersections of the function $-\frac{\Lambda}{3} p^3 + p$ with horizontal lines corresponding to various values of $-2n$. Since the metric coefficients g_{zz} and g_{pp} must remain positive, we require $-\frac{\Lambda}{3} p^3 + p > -2n$. An explicit visualization is given in Fig. 7. The left part applies to $\Lambda > 0$, while the right part applies to $\Lambda < 0$. It can be seen that for $\Lambda > 0$ and $n \geq 0$, the values of p are $p \in (0, p_1)$. For $-\frac{1}{3\sqrt{\Lambda}} < n < 0$, the allowed range is $p \in (p_0, p_1)$ given by two roots of Eq. (58). For $n = -\frac{1}{3\sqrt{\Lambda}}$ the metric degenerates because only one value $p = \frac{1}{\sqrt{\Lambda}}$ is allowed. Finally, there is no solution for $n < -\frac{1}{3\sqrt{\Lambda}}$. In the case $\Lambda < 0$, the situation is much simpler because the function $-\frac{\Lambda}{3} p^3 + p$ monotonously grows from zero. Therefore, for $n \geq 0$ the coordinate p takes the maximal range $(0, \infty)$, while for $n < 0$ its range is restricted to $p \in (p_0, \infty)$.

Interestingly, it is possible to extend the BI metric (57) to include p_i (the roots of g_{zz}) by performing the transformation

$$\rho^2 = 1 + \frac{2n}{p} - \frac{\Lambda}{3} p^2, \quad \sinh \tau = q, \quad \zeta = \frac{1}{2n} z, \quad \varphi = t. \tag{59}$$

TABLE II. Ranges of p and the corresponding ranges of ρ for possible combinations of Λ and n in the BI metric (57). Here $\rho_{\min}$ and $\rho_{\max}$ denote specific minimal and maximal values or ρ.

Λ	n	Range of p	Range of $\rho > 0$
>0	>0	$(0, p_1)$	$(0, \infty)$
>0	<0	(p_0, p_1)	$(0, \rho_{\max})$
<0	>0	$(0, \infty)$	$(\rho_{\min}, \infty)$
<0	<0	(p_0, ∞)	$(0, \infty)$

In fact, for $\Lambda = 0$ this reduces to Eq. (26). The resulting metric is

$$ds^2 = 4n^2[R_1(\rho)(-d\tau^2 + \cosh^2\tau d\varphi^2) + \rho^2 d\zeta^2 + R_2(\rho)d\rho^2], \tag{60}$$

where $R_1(\rho) = \frac{1}{4n^2} p^2(\rho)$, $R_2(\rho) = \frac{1}{4n^2}(np(\rho)^{-2} + \frac{1}{3}\Lambda p(\rho))^{-2}$, with $p(\rho)$ obtained by inverting the relation (59). For $\Lambda = 0$ we recover the metric (27). Relations between the ranges of p and the ranges of $\rho > 0$ are shown in Table II.

B. *BII* metric with Λ

For $\epsilon_2 = -1$ the metric (8) gives

$$ds^2 = -p^2(\epsilon_0 + q^2)dt^2 + \frac{p^2}{\epsilon_0 + q^2}dq^2$$
$$+ \left(-1 + \frac{2n}{p} - \frac{\Lambda}{3} p^2\right)dz^2$$
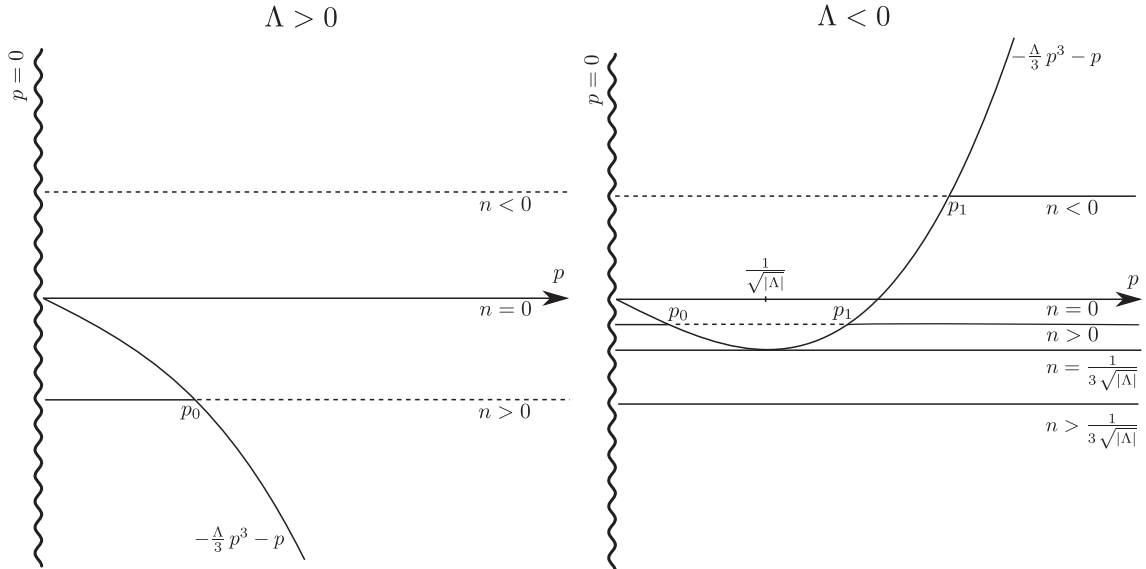$$+ \left(-1 + \frac{2n}{p} - \frac{\Lambda}{3} p^2\right)^{-1}dp^2, \tag{61}$$

FIG. 8. Allowed ranges of p for $\Lambda > 0$ (left) and $\Lambda < 0$ (right) in the *BII* metric (61). They are determined by those parts of the horizonal lines $-2n$ that lie under the curve $-\frac{\Lambda}{3} p^3 - p$.

TABLE III.   Ranges of p and ρ for possible Λ and n in the *BII* metric (61).

Λ	n	Range of p	Range of $\rho > 0$
>0	>0	$(0, p_0)$	$(0, \infty)$
<0	$>\frac{1}{3\sqrt{|\Lambda|}}$	$(0, \infty)$	$(\rho_{\min}, \infty)$
<0	$0 < n < \frac{1}{3\sqrt{|\Lambda|}}$	$(0, p_0), (p_1, \infty)$	$(0, \infty)$
<0	<0	(p_1, ∞)	$(0, \infty)$

where $t, q, z \in \mathbb{R}$ (considering $\epsilon_0 = 1$). The range of p is given by the roots $0 < p_0 < p_1$ of

$$-\frac{\Lambda}{3}p^3 - p + 2n = 0. \tag{62}$$

We plot the allowed ranges of p for different values of Λ and n in Fig. 8. For $\Lambda > 0$, $n > 0$ the range is $p \in (0, p_0)$, while the case $n \leq 0$ is forbidden. For $\Lambda < 0$ the coordinate p has the full range $(0, \infty)$ for any $n > \frac{1}{3\sqrt{|\Lambda|}}$. If $n = \frac{1}{3\sqrt{|\Lambda|}}$ the metric degenerates at $p = \frac{1}{\sqrt{|\Lambda|}}$. If $0 < n < \frac{1}{3\sqrt{|\Lambda|}}$, the metric represents two separate regions $p \in (0, p_0)$ and $p \in (p_1, \infty)$. Finally, if $n \leq 0$ the coordinate p can only take values $p \in (p_1, \infty)$. Notice that $n \leq 0$ is forbidden for the *BII* metrics (28) with $\Lambda = 0$ and (61) with $\Lambda > 0$. In particular, the *BII* metric (61) with $\Lambda < 0$ (and sufficiently large $|\Lambda|$) includes the anti–de Sitter spacetime when $n = 0$.

Again, we can perform its extension to include p_i, in this case by generalizing Eq. (29) to

$$\rho^2 = -1 + \frac{2n}{p} - \frac{\Lambda}{3}p^2, \quad \sinh z = q, \quad \zeta = \frac{1}{2n}z. \tag{63}$$

The extended *BII* metric will then be

$$ds^2 = 4n^2[R_1(\rho)(dz^2 - \cosh^2 z \, dt^2) + \rho^2 d\zeta^2 + R_2(\rho)d\rho^2]. \tag{64}$$

The explicit form of the metric functions $R_1(\rho), R_2(\rho)$ [reducing to Eq. (30) when $\Lambda = 0$] is obtained by using the function $p(\rho)$ that is obtained by inverting Eq. (63). The ranges of $\rho > 0$ corresponding to the allowed ranges of p are shown in Table III.

C. *BIII* metric with Λ

The metric (8) for $\epsilon_2 = 0$ (and, without loss of generality, $\epsilon_0 = 1$) reads

$$ds^2 = -p^2 dt^2 + p^2 dq^2 + \left(\frac{2n}{p} - \frac{\Lambda}{3}p^2\right)dz^2 + \left(\frac{2n}{p} - \frac{\Lambda}{3}p^2\right)^{-1}dp^2, \tag{65}$$

where $t, q, z \in \mathbb{R}$, and the range of p is determined by the roots of

$$-\frac{\Lambda}{3}p^3 + 2n = 0. \tag{66}$$

The results are visualized in Fig. 9. For $\Lambda > 0$, $n > 0$, the allowed range is $p \in (0, p_0)$. As for the *BII* metric, the case $n \leq 0$ is not allowed. When $\Lambda < 0$, $n \geq 0$, the coordinate p varies in the range $(0, \infty)$, while for $n < 0$, it varies in the range (p_0, ∞). Of course, Eq. (66) can be explicitly solved: for $n/\Lambda > 0$, the root is $p_0 = \sqrt[3]{6n/\Lambda}$, while for $n/\Lambda < 0$ there is no positive root. These *BIII* metrics are, in fact, equivalent to the Linet-Tian metric; see Refs. [8,18].
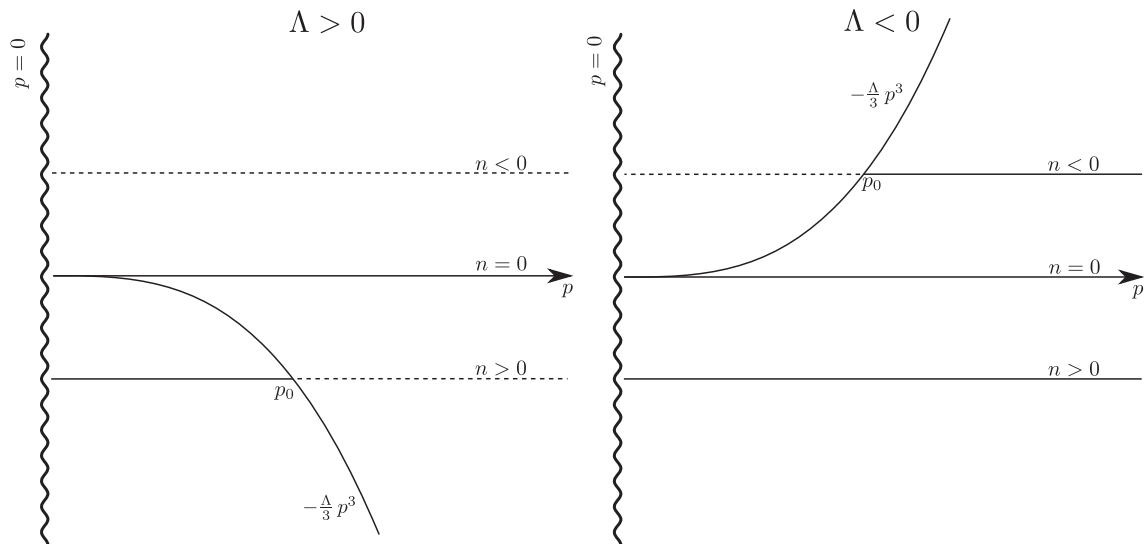

FIG. 9.   Allowed ranges of p for $\Lambda > 0$ (left) and $\Lambda < 0$ (right) in the *BIII* metric (65). They are determined by the root $p_0 = \sqrt[3]{6n/\Lambda}$ of Eq. (66).

TABLE IV.   Ranges of p and ρ for possible Λ and n in the $BIII$ metric (65).

Λ	n	Range of p	Range of $\rho > 0$
>0	>0	$(0, p_0)$	$(0, \infty)$
<0	>0	$(0, \infty)$	$(\rho_{\min}, \infty)$
<0	<0	(p_0, ∞)	$(0, \infty)$

We can also make an extension to include p_0 (which does not have a counterpart for the $\Lambda = 0$ case because there are no roots of g_{zz}). Such an extension is achieved by

$$\rho^2 = \frac{2n}{p} - \frac{\Lambda}{3} p^2, \qquad \zeta = \frac{1}{2n} z, \tag{67}$$

and the extended $BIII$ metric takes the form

$$ds^2 = 4n^2[R_1(\rho)(-dt^2 + dq^2) + \rho^2 d\zeta^2 + R_2(\rho)d\rho^2], \tag{68}$$

where $R_1(\rho)$, $R_2(\rho)$ are evaluated by inverting Eq. (67). The allowed ranges of p and the corresponding ranges of ρ are summarized in Table IV.

VII. GLOBAL STRUCTURE AND PHYSICAL INTERPRETATION: TACHYONS IN (ANTI–)DE SITTER SPACETIME

The metric describing both internal Regions 1 and 2 around the tachyonic source is the AII metric with Λ, namely

$$ds^2 = \sigma^2(d\vartheta^2 + \sinh^2\vartheta d\varphi^2) + \left(1 - \frac{2M}{\sigma} + \frac{\Lambda}{3}\sigma^2\right)dz^2$$
$$- \left(1 - \frac{2M}{\sigma} + \frac{\Lambda}{3}\sigma^2\right)^{-1}d\sigma^2, \tag{69}$$

while the external Region 3 is described by the BI metric with Λ

$$ds^2 = p^2(-d\tau^2 + \cosh^2\tau d\varphi^2) + \left(1 - \frac{2M}{p} - \frac{\Lambda}{3}p^2\right)dz^2$$
$$+ \left(1 - \frac{2M}{p} - \frac{\Lambda}{3}p^2\right)^{-1}dp^2, \tag{70}$$

generalizing Eqs. (32) and (33), assuming $M > 0$.

A. Weak-field limit and distinct regions

As for $\Lambda = 0$, the key point is to consider the weak-field limit $M \to 0$ of Eqs. (69) and (70), in which case the curvature singularities at $\sigma = 0$ and $p = 0$ disappear and the spacetimes (being then vacuum and conformally flat) can readily be interpreted as an (anti–)de Sitter universe in which the *test tachyonic source* (located at $\sigma = 0$ and $p = 0$) moves with infinite speed.

The trajectory of such a tachyon on the hyperboloid (45) can be determined using the corresponding five-dimensional parametrizations. The internal AII metric (69) with $M = 0$ and $\Lambda > 0$ is de Sitter spacetime covered by

$$Z_0 = \pm\sigma\cosh\vartheta,$$
$$Z_1 = \sigma\sinh\vartheta\cos\varphi,$$
$$Z_2 = \sigma\sinh\vartheta\sin\varphi,$$
$$Z_3 = \sqrt{\sigma^2 + a^2}\cos\phi,$$
$$Z_4 = \sqrt{\sigma^2 + a^2}\sin\phi, \tag{71}$$

which is actually Eq. (52) with $p = \sigma > 0$, $q = \pm\cosh\vartheta$ and $t = z \equiv a\phi$. The coordinate singularity at $\sigma = 0$ with ϑ finite, localizing the test tachyon, thus corresponds to the trajectory

$$Z_0 = 0, \qquad Z_1 = 0 = Z_2,$$
$$Z_3 = a\cos\phi,$$
$$Z_4 = a\sin\phi. \tag{72}$$

Unlike the tachyon in Minkowski space whose trajectory is given by the straight line (36), which is the Z axis, this tachyon *runs at infinite speed around the neck of the de Sitter hyperboloid*, which is the smallest possible circle $Z_3^2 + Z_4^2 = a^2$ in such a closed universe; see the left part of Fig. 10.

The same is true for the external BI metric (70) with $M = 0$ and $\Lambda > 0$. Indeed, the corresponding parametrization is

$$Z_0 = p\sinh\tau,$$
$$Z_1 = p\cosh\tau\cos\varphi,$$
$$Z_2 = p\cosh\tau\sin\varphi,$$
$$Z_3 = \sqrt{a^2 - p^2}\cos\phi,$$
$$Z_4 = \sqrt{a^2 - p^2}\sin\phi, \tag{73}$$

which is equivalent to Eq. (55) with $q = \sinh\tau$, $t = \varphi$ and $z = a\phi$. Setting $p = 0$ at finite τ, we obtain again the tachyonic trajectory (72).

For $\Lambda < 0$ the tachyonic trajectory is different. The anti–de Sitter hyperboloid (45) with $\epsilon = -1$ is parametrized in the form of the (weak-field limit of the) AII metric (69) as

$$Z_0 = \pm\sigma\cosh\vartheta,$$
$$Z_1 = \sigma\sinh\vartheta\cos\varphi,$$
$$Z_2 = \sigma\sinh\vartheta\sin\varphi,$$
$$Z_3 = \pm\sqrt{a^2 - \sigma^2}\sinh(z/a),$$
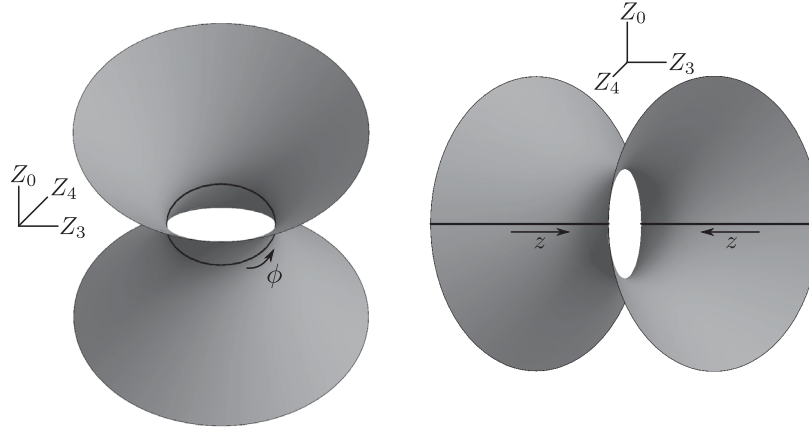$$Z_4 = \pm\sqrt{a^2 - \sigma^2}\cosh(z/a), \tag{74}$$

FIG. 10. Motion of the infinitely fast test tachyon in (anti–)de Sitter background space. For $\Lambda > 0$, the tachyon runs with infinite speed in a closed circle around the neck of the de Sitter hyperboloid (left). For $\Lambda < 0$, there are two tachyons running along two hyperbolic lines on opposite sides, corresponding to the signs $\pm$ in Eq. (75), of the anti–de Sitter hyperboloid (right).

cf. Eq. (53). The test tachyon trajectory given by $\sigma = 0$ with ϑ finite is thus located at

$$Z_0 = 0, \qquad Z_1 = 0 = Z_2,$$
$$Z_3 = \pm a \sinh(z/a),$$
$$Z_4 = \pm a \cosh(z/a). \tag{75}$$

There are thus *two* tachyons *moving at infinite speed along main hyperbolic lines* $Z_4^2 - Z_3^2 = a^2$ *on opposite sides of the anti–de Sitter hyperboloid*, as illustrated in the right part of Fig. 10. If the hyperboloid is unfolded into the covering space, there would be *infinitely many tachyon trajectories* (the tachyons would periodically appear, moving back and forth in the universe).

The same result is obtained for the *BI* metric (70), which for $\Lambda < 0$ corresponds to

$$Z_0 = p \sinh \tau,$$
$$Z_1 = p \cosh \tau \cos \varphi,$$
$$Z_2 = p \cosh \tau \sin \varphi,$$
$$Z_3 = \pm \sqrt{a^2 + p^2} \sinh(z/a),$$
$$Z_4 = \pm \sqrt{a^2 + p^2} \cosh(z/a) \tag{76}$$

[see Eq. (55)]. For $p = 0$ and finite τ, we recover the same tachyonic trajectory (75).

B. Mach-Cherenkov shock wave separating the *AII* and *BI* metrics

In the weak-field limit, the pair of metrics (69) and (70) together cover the full (anti–)de Sitter universe. The internal Regions 1 and 2 are localized at $Z_0^2 > Z_1^2 + Z_2^2$ with $Z_0 > 0$ and $Z_0 < 0$, respectively. They are represented

by two *AII* metrics (69). The complementary external Region 3 represented by a single *BI* metric (70) is localized at $Z_0^2 < Z_1^2 + Z_2^2$.

These regions are *separated by the surface* $Z_1^2 + Z_2^2 = Z_0^2$, with Z_3 arbitrary such that $Z_3^2 = \epsilon(a^2 - Z_4^2)$, corresponding to the singularities $\sigma = 0$, $\vartheta = \infty$ and $p = 0$, $\tau = \infty$, respectively. This surface represents the *Mach-Cherenkov shocks*, i.e., the *contracting one for* $Z_0 < 0$ given by $\sqrt{Z_1^2 + Z_2^2} = -Z_0$ and the *expanding one for* $Z_0 > 0$ given by $\sqrt{Z_1^2 + Z_2^2} = Z_0$. As in the case of the Minkowski background, visualized in Fig. 1, it is locally a *contracting/expanding cylinder around the superluminal tachyonic source*. However, in the $\Lambda > 0$ case, this cylinder is "wrapped" around the circular trajectory (72) in closed de Sitter space, so that topologically and also geometrically it is a *toroidal surface*. For $\Lambda < 0$, instead, there are *two infinite cylinders* around Eq. (75) on opposite sides of the anti–de Sitter hyperbolic space; see Fig. 10.

The position of these shock surfaces, separating the *AII* and *BI* regions, is shown in Fig. 11 for typical three-dimensional sections (given by three distinct values of Z_4) through de Sitter space, and in Fig. 12 for anti–de Sitter space.

It is also interesting to plot the Mach-Cherenkov shock wave and tachyon position in *compactified conformal diagrams* representing the global structure of (anti–)de Sitter background space. Such Penrose conformal diagrams are specific parts of the Einstein static universe, represented as a solid cylinder with conformal time η plotted vertically and spatial angular coordinates χ, θ, ϕ on the 3-sphere plotted horizontally; see e.g., Ref. [4]. Details of the exact construction of such diagrams, describing the conformal structure of (anti–)de Sitter space in the coordinates which correspond to the weak-field limit of the *B* metrics, can be found in our previous article [7]. Using these results (in particular,
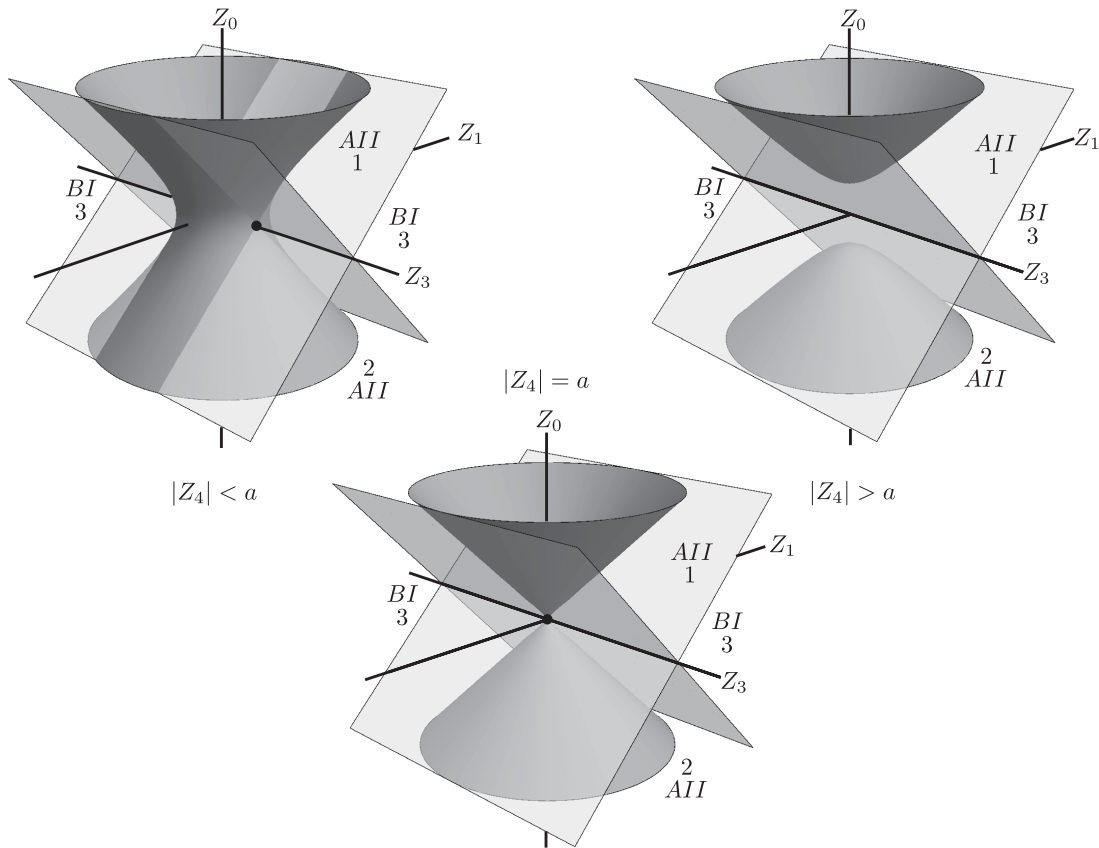
FIG. 11.   Separation of the background de Sitter space into Regions 1, 2 and 3, covered by the AII and BI metrics, for $Z_2 = 0$ and $|Z_4| < a$ (upper left part), $|Z_4| > a$ (upper right part) and $|Z_4| = a$ (lower part). For $|Z_4| < a$ the separation surface $Z_1^2 + Z_2^2 = Z_0^2$ cuts the de Sitter hyperboloid, for $|Z_4| = a$ it is tangent to it, and for $|Z_4| > a$ this surface does not intersect the hyperboloid. Because the coordinate Z_4 is suppressed here, the tachyon motion is not visualized very well: in this section, it corresponds just to two points at the intersection of the Z_3 axis with the hyperboloid when $|Z_4| < a$, and one point when $|Z_4| = a$. The tachyon motion is better seen in Fig. 10 where both nontrivial coordinates Z_3 and Z_4 are visible.
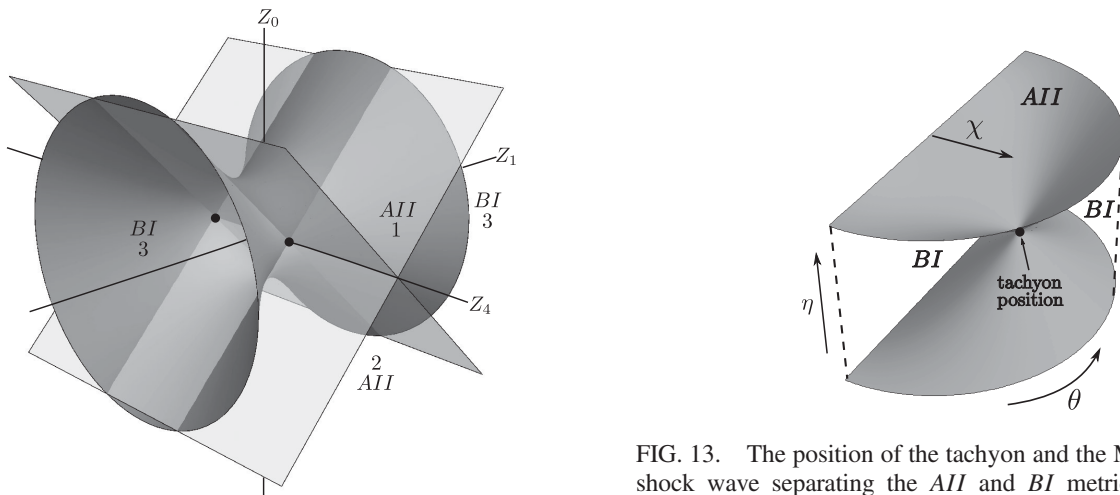

FIG. 12.   Separation of the background anti–de Sitter space into Regions 1, 2 and 3 for the section $Z_2 = 0$, $Z_3 = $ const. Unlike for de Sitter space, visualized in Fig. 11, this picture looks qualitatively the same for any value of Z_3. The motion of the tachyon is better seen in Fig. 10.

FIG. 13.   The position of the tachyon and the Mach-Cherenkov shock wave separating the AII and BI metrics in the global conformal representation of de Sitter spacetime for arbitrary $\phi = $ const. Since the angular coordinate $\phi \in [0, 2\pi)$ is suppressed, the tachyon is visible here only as a single point at $\eta = \frac{\pi}{2}, \chi = \frac{\pi}{2}, \theta = \frac{\pi}{2}$. The bottom spacelike surface $\eta = 0$ is the past conformal infinity $\mathcal{I}^-$ of the de Sitter universe, while the top surface $\eta = \pi$ is its future conformal infinity $\mathcal{I}^+$.
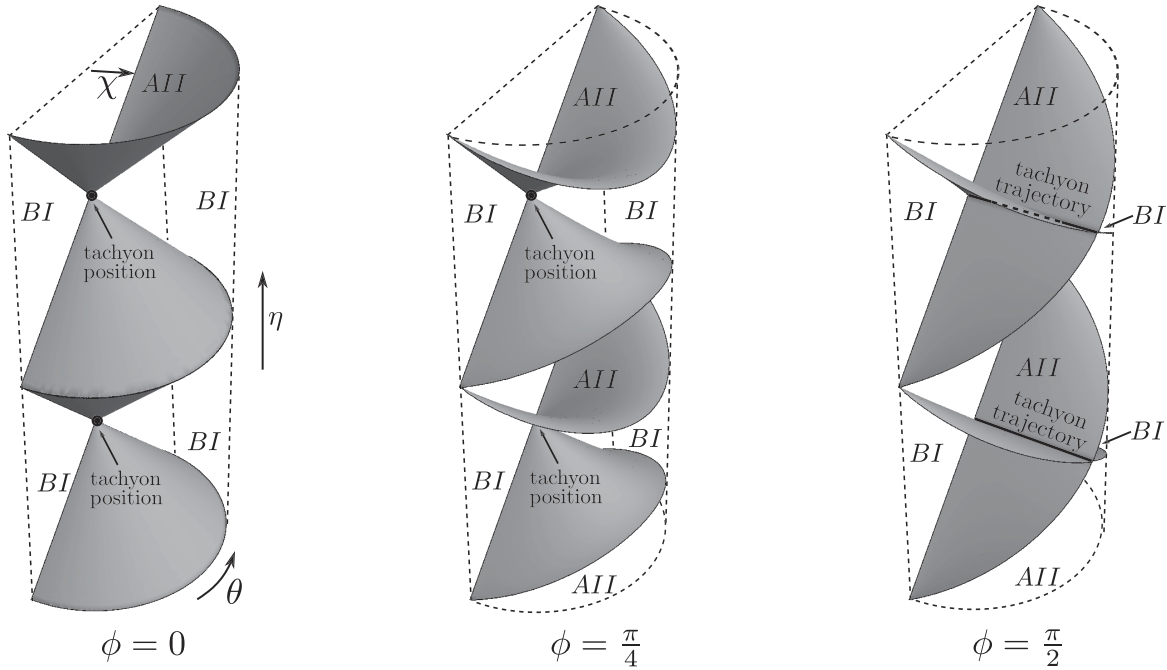
FIG. 14. The position of the tachyon and the Mach-Cherenkov shock wave separating the *AII* and *BI* metrics in the global conformal representation of anti–de Sitter spacetime for $\phi = 0$ (left), $\phi = \frac{\pi}{4}$ (middle) and $\phi = \frac{\pi}{2}$ (right). Unlike the case $\Lambda > 0$ shown in Fig. 13, these conformal diagrams depend on ϕ. In the unfolded covering space, the tachyon periodically reappears in time, namely at $\eta = \frac{\pi}{2} + k\pi$, $k \in \mathbb{Z}$. Its full trajectory is only visible in the section $\phi = \frac{\pi}{2}$. The outer cylindrical boundary $\chi = \frac{\pi}{2}$ is the null conformal infinity $\mathcal{I}$ of the anti–de Sitter universe.

Fig. 4 and Fig. 13 of Ref. [7]) we plot here the conformal diagram for de Sitter space in Fig. 13, and for anti–de Sitter space in Fig. 14.

C. Boosted metrics with $\Lambda \neq 0$

Following the idea outlined in Ref. [7], it is useful to perform a *boost which slows the tachyonic source* from infinite speed to some finite speed $v > 1$. This enables us to better illustrate its motion and the generated Mach-Cherenkov conical shock waves in a (anti–)de Sitter

universe, analogously to the flat background case shown in Fig. 4. Such a boost must be performed in the five-dimensional coordinates of Eqs. (45) and (46). Choosing the spatial Z_3 direction, it reads

$$Z_0 = \frac{vZ_0' - Z_3'}{\sqrt{v^2 - 1}}, \qquad Z_3 = \frac{vZ_3' - Z_0'}{\sqrt{v^2 - 1}}, \qquad (77)$$

cf. Eq. (21). The tachyon moving along $Z_1 = 0 = Z_2$ at $Z_0 = 0$ [see Eqs. (72) and (75)] is then located at $Z_3' = vZ_0'$, and the shock wave surface $Z_1^2 + Z_2^2 = Z_0^2$ becomes
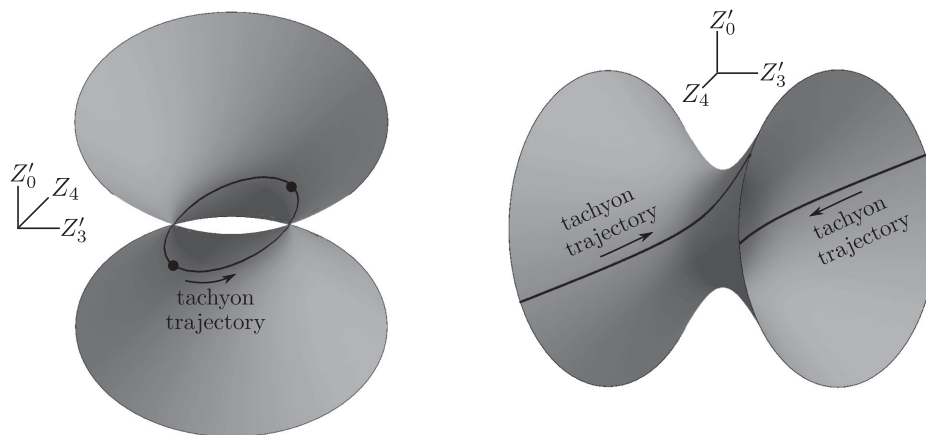

FIG. 15. Motion of a slowed tachyon in de Sitter (left) and anti–de Sitter (right) background space in boosted coordinates. Its trajectory is given by $Z_3'/Z_0' = v > 1$ and $Z_1 = 0 = Z_2$.
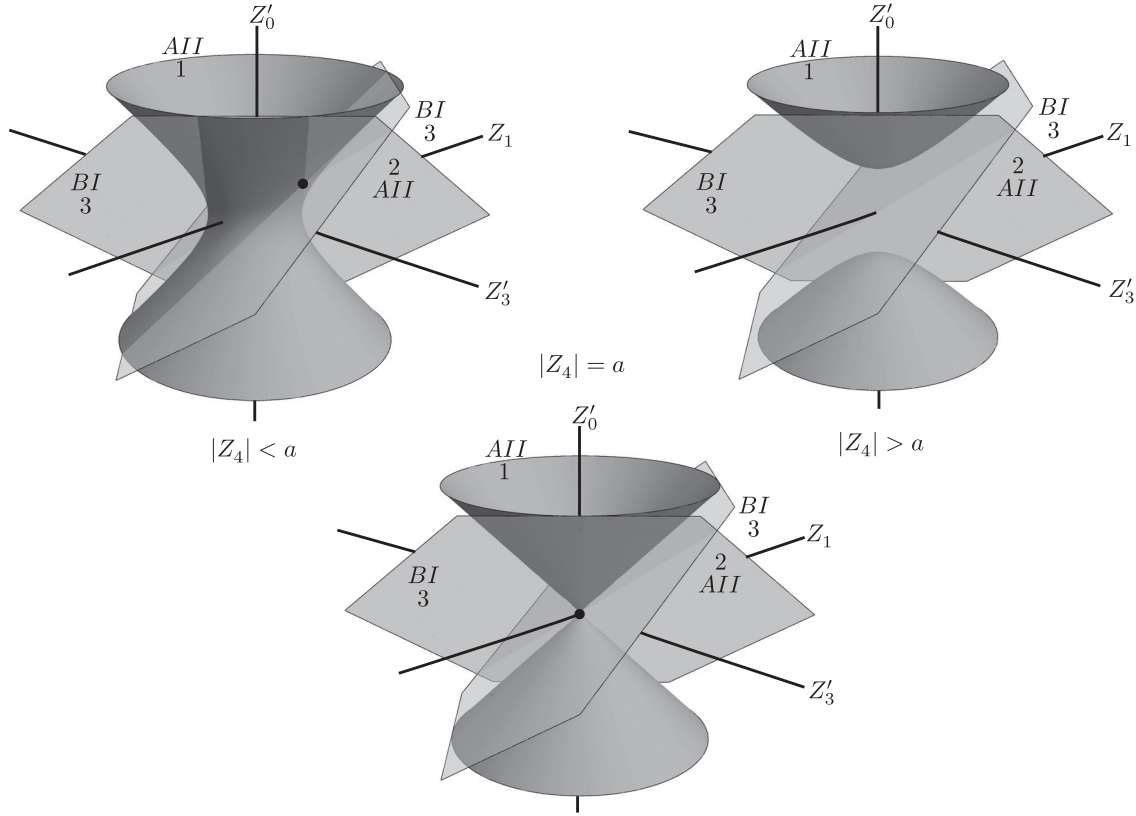
FIG. 16. Separation of the de Sitter universe into Regions 1, 2 and 3 in the boosted coordinates for $|Z_4| < a$ (upper left part), $|Z_4| > a$ (upper right part) and $|Z_4| = a$ (lower part), with $Z_2 = 0$. The intersections of these separation boundaries with the hyperboloid in the upper left part give the position of the Mach-Cherenkov shock cones in the de Sitter universe. The tachyon is always located at their joint vertex at $Z_1 = 0 = Z_2$.

$$Z_1^2 + Z_2^2 = \frac{(vZ_0' - Z_3')^2}{v^2 - 1}. \qquad (78)$$

The *trajectory* of this slowed tachyon in a (anti–)de Sitter universe is illustrated in Fig. 15.

Such a motion in de Sitter space admits two interpretations. The first is that the tachyon moves forward in time from the initial point (starting at $Z_0' = -Z_{0\,\mathrm{max}}'$) to the final point (reaching it at $Z_0' = +Z_{0\,\mathrm{max}}'$), and then travels *backwards in time* to the initial point, also at a speed faster than light. The second is that the tachyon moves from the initial to the final point along *both trajectories* (recall that there is not a unique geodesic between two events in pseudo-Riemannian geometry). The specific value $Z_{0\,\mathrm{max}}'$ can be evaluated. Substituting the conditions $Z_1 = 0 = Z_2$, $Z_3' = vZ_0'$ into the boosted form of Eq. (45), namely $-Z_0'^2 + Z_1^2 + Z_2^2 + Z_3'^2 + Z_4^2 = a^2$, we obtain $Z_0'^2 = (a^2 - Z_4^2)/(v^2 - 1)$. This explicitly determines the position of the tachyon on the de Sitter hyperboloid as a function of time Z_0'. Extreme values of Z_0' arise when $Z_4 = 0$, yielding

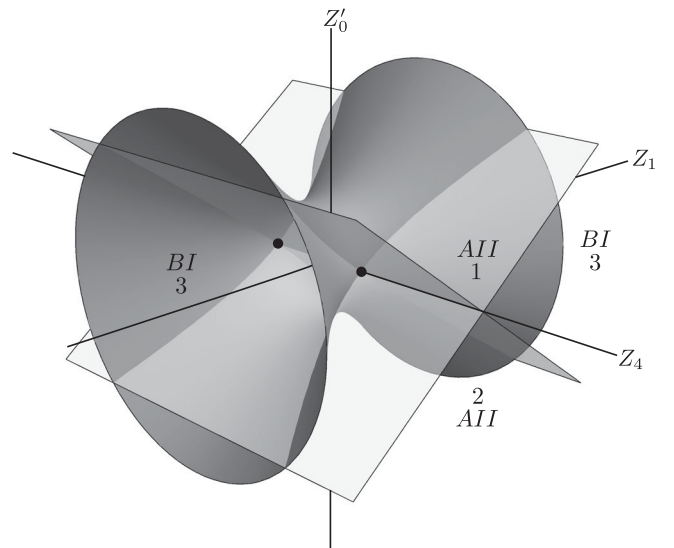$$Z_{0\,\mathrm{max}}' = \frac{a}{\sqrt{v^2 - 1}}. \qquad (79)$$

FIG. 17. Separation of the anti–de Sitter universe into Regions 1, 2 and 3 in the boosted coordinates. Notice that Regions 1 and 2, covered by the *AII* metrics, are larger, whereas Region 3 covered by the *BI* metric is smaller, compared to Fig. 12 (i.e., without the boost).

In anti–de Sitter space there are *two tachyons*, each moving faster than light on opposite sides of the universe; see the right part of Fig. 15. "Unfolding" the hyperboloid, there would be just one tachyon oscillating between $Z'_3, Z_4 = \pm\infty$, that is "bouncing off" the conformal infinity.

Regions 1, 2 and 3, separated by the conical shock wave surface (78) in the *boosted coordinates of de Sitter space*, are shown in Fig. 16. At any time Z'_0, these separation boundaries localize the Mach-Cherenkov shock on the hyperboloid, namely the *rear expanding cone* and the *forward contracting cone*. Analogously to the situation shown in Fig. 4, the tachyon is always located at the intersection of these two cones at $Z_1 = 0 = Z_2$.

Similarly, in Fig. 17 we visualize these separation boundaries and the corresponding two conical shocks in the *boosted form of anti–de Sitter space*.

Finally, it is illustrative to visualize the de Sitter spacetime, together with the actual position of the Mach-Cherenkov shocks, in *spatial sections* given by Z_1, Z_2, Z'_3

(with a fixed value of $Z_4 < a$). This is done in Fig. 18 for five different times $Z'_0 = \text{const}$. In any such section, the de Sitter spatial geometry is a 3-sphere, represented here as a 2-sphere because one spatial dimension is suppressed in this plot. As a function of Z'_0, this *de Sitter sphere contracts to a minimal size at $Z'_0 = 0$ and then reexpands*. The shock surface given by Eq. (78) has the form of two cones, with the tachyon located at their joint vertex. The position of the Mach-Cherenkov shocks in the de Sitter universe is given here by the *circular intersection of these cones with each sphere*. There are two shocks: the forward shock and the rear one. Recall that these shocks separate the internal Regions 1 and 2 (with the *AII* metric) from the external Region 3 (endowed with the *BI* metric).

The top left part of Fig. 18 shows the situation in a generic time $Z'_0 < -Z'_{0\,\text{max}}$, in which case both the shocks are contracting from the equator of the spherical de Sitter space, approaching the north pole and the south pole (both located at $Z_1 = 0 = Z_2$), respectively. At the special time
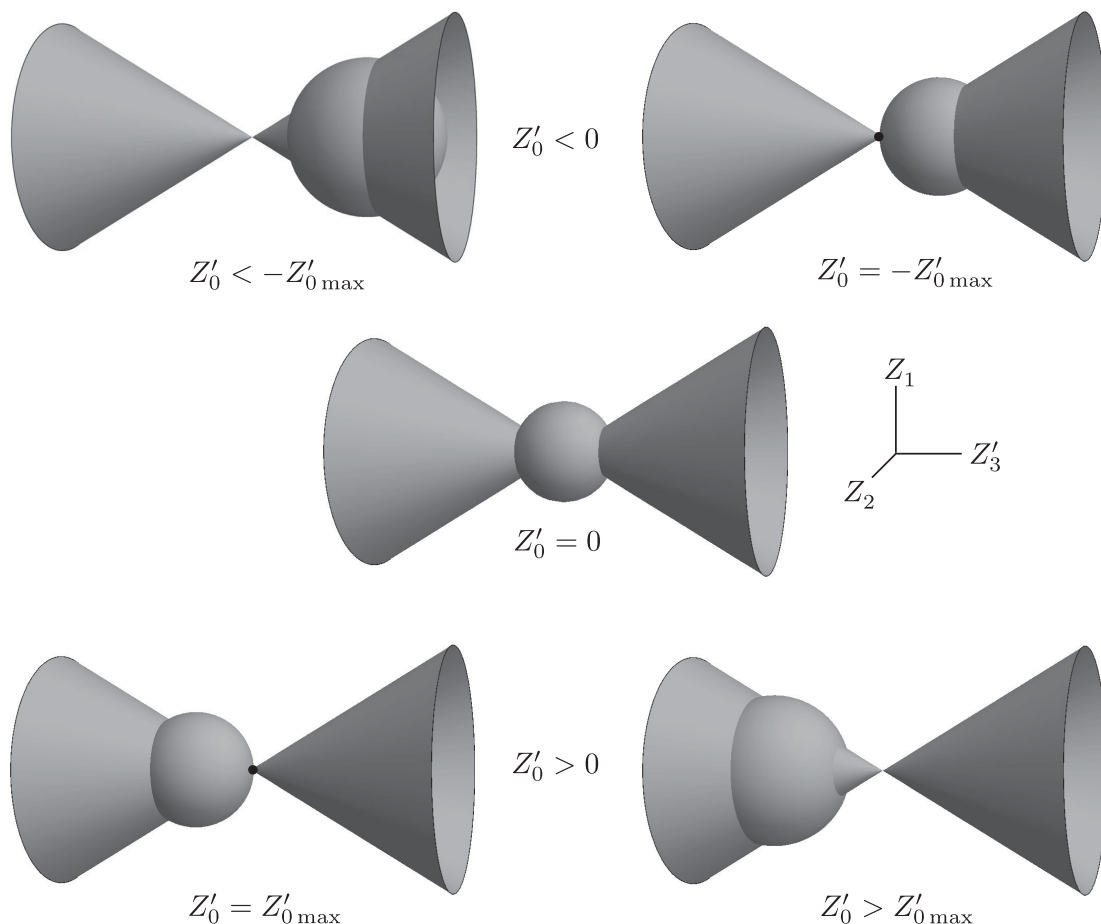

FIG. 18. A time sequence visualizing the de Sitter universe—in this section Z_1, Z_2, Z'_3 represented as a sphere—at five different times $Z'_0 = \text{const}$ (and fixed $Z_4 < a$). The universe contracts, reaches its minimal size at $Z'_0 = 0$, and then reexpands. The intersections of the sphere with the cones give the actual position of the two Mach-Cherenkov shocks in the universe. For $Z'_0 < -Z'_{0\,\text{max}}$ both shocks are contracting on the sphere towards its poles, while for $Z'_0 > Z'_{0\,\text{max}}$ they are both expanding from the poles. The tachyon is always located at the joint vertex of the cones. Analogous pictures apply to the anti–de Sitter universe expressed in global static coordinates because the 2-spaces of constant T and r are also spheres; see the metric (5.4) in Ref. [4].

$Z'_0 = -Z'_{0\,\text{max}}$, shown in the top right part, the tachyon occurs at the north pole of the space when the first contracting shock reaches it, crosses it, and starts to reexpand. The second shock in the southern hemisphere continues to contract towards the south pole. At $Z'_0 = 0$ (see the middle part of Fig. 18) the situation is fully symmetric: the closed de Sitter universe has a minimal radius, both shock waves are of the same size, and they are located symmetrically with respect to the equator. For $Z'_0 > 0$, the situation is complementary to the top part of the figure. The bottom left part shows the tachyon located at the south pole at time $Z'_0 = Z'_{0\,\text{max}}$ when the second contracting shock has just shrinked to zero and starts to reexpand from the south pole, while the first shock had been already expanding from the north pole. A generic situation at a time $Z'_0 > Z'_{0\,\text{max}}$ is shown in the bottom right part of Fig. 18, with two expanding shocks in the expanding de Sitter universe, both approaching the equator.

VIII. CONCLUSIONS

We have presented and analyzed the classes of *A* and *B* metrics with an arbitrary value of the cosmological constant. While the famous Schwarzschild–(anti–)de Sitter spacetime (which is the *AI* metric) represents the spherically symmetric gravitational field of a static massive source, the *AII* and *BI* metrics describe specific parts of the field of a superluminal source, i.e., a tachyon moving along the axis of symmetry. In fact, all three families of metrics are related by an appropriate boost (admitting speeds $v > 1$).

We have studied the weak-field limit, analytic extensions, and global structure of these spacetimes. We have demonstrated that the full gravitational field of a tachyon in a Minkowski or (anti–)de Sitter universe can be obtained by combining a pair of *AII* metrics with a single *BI* metric. The former represent the contracting/expanding interior regions while the latter represents an exterior region with respect to the separation boundary which is the contracting/expanding Mach-Cherenkov shock wave. This structure of the "composite spacetime," yielding the complete gravitational field of a tachyonic source moving with any superluminal speed in a Minkowski, de Sitter or anti–de Sitter universe, has been analyzed and visualized in numerous pictures.

In fact, the present work is the third paper in our recent series which we have devoted to a deeper geometric, algebraic, and physical investigation of a large family on nonexpanding Plebański-Demiański spacetimes. This whole family, generalizing the original *B* metrics of Ref. [1], was described and its free parameters were identified and studied in our work [8]. A thorough investigation of the character of the corresponding background coordinates for de Sitter and anti–de Sitter universes was presented in Ref. [7]. We hope that, together with this third complementary paper, we have thus provided an extensive survey and review of this simple yet interesting family of exact solutions of Einstein's field equations.

[1] J. Ehlers and W. Kundt, Exact solutions of the gravitational field equations, in *Gravitation: An Introduction to Current Research* (Wiley, New York, 1962), pp. 49–101.

[2] W. Kinnersley and M. Walker, Uniformly accelerating charged mass in general relativity, Phys. Rev. D **2,** 1359 (1970).

[3] H. Stephani, D. Kramer, M. MacCallum, C. Hoenselaers, and E. Herlt, *Exact Solutions of Einstein's Field Equations*, 2nd ed. (Cambridge University Press, Cambridge, England, 2003).

[4] J. B. Griffiths and J. Podolský, *Exact Space-Times in Einstein's General Relativity* (Cambridge University Press, Cambridge, England, 2009).

[5] K. Schwarzschild, Über das gravitationsfeld eines massenpunktes nach der Einsteinschen theorie, Sitzungsber. Preuss. Akad. Wiss. Phys. Math. Kl. 189 (1916); Golden Oldie: On the gravitational field of a mass point according to Einstein's theory, Gen. Relativ. Gravit. **35,** 951 (2003).

[6] F. Kottler, Über die physikalischen Grundlagen der Einsteinschen gravitations theorie, Ann. Phys. (Berlin) **361,** 401 (1918).

[7] J. Podolský and O. Hruška, Yet another family of diagonal metrics for de Sitter and anti-de Sitter spacetimes., Phys. Rev. D **95,** 124052 (2017).

[8] J. Podolský, O. Hruška, and J. B. Griffiths, Non-expanding Plebański–Demiański space-times, Classical Quantum Gravity **35,** 165011 (2018).

[9] J. F. Plebański and M. Demiański, Rotating charged and uniformly accelerating mass in general relativity, Ann. Phys. (N.Y.) **98,** 98 (1976).

[10] J. B. Griffiths and J. Podolský, A new look at the Plebański–Demiański family of solutions, Int. J. Mod. Phys. D **15,** 335 (2006).

[11] O. Hruška, The study of exact spacetimes with a cosmological constant, Diploma thesis, Charles University, 2015.

[12] A. Peres, Gravitational field of a tachyon, Phys. Lett. A **31**, 361 (1970).

[13] L. S. Schulman, Gravitational shock waves from tachyons, Nuovo Cimento B **2**, 38 (1971).

[14] J. R. Gott, Tachyon singularity: A spacelike counterpart of the Schwarzschild black hole, Nuovo Cimento B **22**, 49 (1974).

[15] M. Hotta and M. Tanaka, Shock-wave geometry with non-vanishing cosmological constant, Classical Quantum Gravity **10**, 307 (1993).

[16] J. Podolský and J. B. Griffiths, Impulsive gravitational waves generated by null particles in de Sitter and anti-de Sitter backgrounds, Phys. Rev. D **56**, 4756 (1997).

[17] J. Podolský and J. B. Griffiths, Boosted static multipole particles as sources of impulsive gravitational waves, Phys. Rev. D **58**, 124024 (1998).

[18] J. B. Griffiths and J. Podolský, The Linet–Tian solution with a positive cosmological constant in four and higher dimensions, Phys. Rev. D **81**, 064015 (2010).